HHS Public Access

Author manuscript

Sci Transl Med. Author manuscript; available in PMC 2022 December 13.

Published in final edited form as:

Sci Transl Med. 2022 May 25; 14(646): eabl8753. doi:10.1126/scitranslmed.abl8753.

Schwann cells in the subcutaneous adipose tissue have neurogenic potential and can be used for regenerative therapies

Rhian Stavely,

Ryo Hotta,

Nicole Picard,

Ahmed A Rahman,

Weikang Pan,

Sukhada Bhave,

Meredith Omer,

Wing Lam N. Ho,

Richard A. Guyer,

Allan M. Goldstein[*]

Department of Pediatric Surgery, Massachusetts General Hospital, Harvard Medical School, Boston, MA 02114, USA.

Abstract

Stem cell therapies for nervous system disorders are hindered by a lack of accessible autologous sources of neural stem cells (NSCs). In this study, neural crest–derived Schwann cells are found to populate nerve fiber bundles (NFBs) residing in mouse and human subcutaneous adipose tissue (SAT). NFBs containing Schwann cells were harvested from mouse and human SAT and cultured in vitro. During in vitro culture, SAT-derived Schwann cells remodeled NFBs to form neurospheres and exhibited neurogenic differentiation potential. Transcriptional profiling

[*]Corresponding author. amgoldstein@partners.org.

Author contributions: R.S. designed the experiments; conducted cell culture, flow cytometry, immunohistochemistry, imaging and associated analysis, and visualization of the data; and wrote the original draft of the manuscript. R.H. designed cell administration procedures in vivo and ex vivo, conducted radiographic assays, and contributed to the writing of the manuscript. N.P. performed immunohistochemical studies, PCR, and animal generation and contributed to the writing of the manuscript. A.A.R. designed and conducted electric field stimulation and force contraction experiments, performed associated data analysis and visualization, and contributed to the writing of the manuscript. W.P. performed cell administration procedures and contributed to the writing of the manuscript. S.B. performed optimization of calcium imaging experiments and contributed to the writing of the manuscript. M.O. performed immunohistochemical studies and animal generation and contributed to the writing of the manuscript. W.L.N.H. performed immunohistochemical studies and animal generation and contributed to the writing of the manuscript. R.A.G. contributed to animal generation, RNA-seq experiments, and the writing of the manuscript. A.M.G. provided funding, designed the experiments, and wrote the original draft of the manuscript.

Competing interests: The authors declare that they have no competing interests.

SUPPLEMENTARY MATERIALS

www.science.org/doi/10.1126/scitranslmed.abl8753

Materials and Methods

Figs. S1 to S6

Table S1

Movies S1 and S2

Data files S1 and S2

References (44–59)

View/request a protocol for this paper from *Bio-protocol*.

determined that the acquisition of these NSC properties can be attributed to dedifferentiation processes in cultured Schwann cells. The emerging population of cells were termed SAT-NSCs because of their considerably distinct gene expression profile, cell markers, and differentiation potential compared to endogenous Schwann cells existing in vivo. SAT-NSCs successfully engrafted to the gastrointestinal tract of mice, migrated longitudinally and circumferentially within the muscularis, differentiated into neurons and glia, and exhibited neurochemical coding and calcium signaling properties consistent with an enteric neuronal phenotype. These cells rescued functional deficits associated with colonic aganglionosis and gastroparesis, indicating their therapeutic potential as a cell therapy for gastrointestinal dysmotility. SAT can be harvested easily and offers unprecedented accessibility for the derivation of autologous NSCs from adult tissues. Evidence from this study indicates that SAT-NSCs are not derived from mesenchymal stem cells and instead originate from Schwann cells within NFBs. Our data describe efficient isolation procedures for mouse and human SAT-NSCs and suggest that these cells have potential for therapeutic applications in gastrointestinal motility disorders.

INTRODUCTION

Treating nervous system disorders with regenerative cell therapies requires autologous neural progenitors from an accessible source. The subcutaneous adipose tissue (SAT) contains a reservoir of adipose stem cells that can be readily obtained, such as by minimally invasive liposuction procedures (1). These cells have been examined in over 270 clinical trials for a variety of diseases, demonstrating favorable patient safety profiles (2). Adipose stem cells include a neural stem cell (NSC) population that offers a potential treatment option for neurological diseases (3). The prevailing hypothesis has been that these SAT-derived NSCs (SAT-NSCs) arise from mesenchymal stem cells (MSCs) that transdifferentiate to a neurogenic lineage. However, that hypothesis is controversial given the occurrence of stress-induced cytoskeletal and gene expression abnormalities observed in vitro, cell fusion and leakage of cell tracing dyes after in vivo administration, and a lack of functional evidence consistent with the properties of neurons (4–7). It has also been postulated that a separate uncharacterized progenitor population contaminating MSC cultures may explain their neurogenic potential (5). SAT-NSCs comprise only a small population of adipose stem cells with an unknown physiological niche. Despite almost two decades of research, there is a lack of protocols to isolate, expand, and purify SAT-NSCs that would enable examination of their properties and evaluation of their therapeutic utility as a cellular therapy in preclinical models.

NSCs are most commonly sourced from neural tissue such as the central nervous system, the enteric nervous system (ENS) of the gut (8, 9), or from genetically modified induced pluripotent stem cells (iPSCs) (10); however, concerns remain over the use of the latter in humans because of their tumorigenic potential (11). Emerging evidence has shown that adipose tissue contains its own complex nervous system consisting of sympathetic and sensory innervation (12). The entirety of the peripheral nervous system is the progeny of WNT1-expressing cells of the embryonic neural crest (NC). This includes the ENS, autonomic neurons, and Schwann cell precursors that provide peripheral glial cells (13). Counterintuitive to their name, however, embryonic Schwann cell precursors represent

multipotent stem cells that migrate along embryonic nerve fibers and contribute to glial and nonglial cell populations, including melanocytes, neuroendocrine chromaffin cells, enteric neurons, sympathetic neurons, and MSCs from the bone marrow, depending on local environmental cues (14). However, no equivalent progenitors are known to exist postnatally in the nerve fiber niche (13, 14). Schwann cells in the adult are known to acquire characteristics of dedifferentiated cells in response to injury and *Mycobacterium leprae* infection (15, 16). Furthermore, Schwann cells have been demonstrated to give rise to enteric neurons postnatally (17, 18), suggesting they retain neuronal progenitor properties and offer a potential source of NSCs for regenerative therapies.

In the present study, we show that NC-derived Schwann cells in the SAT have gliogenic and neurogenic potential, consistent with SAT-NSCs. Moreover, our data suggest that these cells might be the only cell population in the SAT with this property. These cells are distinct from adipose-derived MSCs and reside within the local nervous system niche of the SAT. In addition, we present methods for their enrichment from nerve fiber bundles (NFBs) in mice and humans. After transplantation into the gastrointestinal tract, SAT-NSCs efficiently engraft, migrate within the muscularis layer, and differentiate into enteric neurons and glia. Moreover, transplantation of these cells into mouse models of gastroparesis and Hirschsprung disease (HSCR) improved gastrointestinal function, indicating that SAT-NSCs offer a source of autologous NSCs that could be used for treating ENS disorders.

RESULTS

NC-derived Schwann cells reside in NFBs coursing through the SAT

The NC gives rise to all peripheral neurons and glial cells, including Schwann cells. The constituents of NC-derived structures and Schwann cells in the posterior subcutaneous fat pads were examined in $Plp1^{GFP}$;Wnt1::Cre;$ROSA26^{tdTomato}$ ($Plp1^{GFP}$;Wnt1-tdT) mice, whereby green fluorescent protein (GFP) expression is actively driven by the *Plp1* promoter ($Plp1^{GFP+}$), and NC-derived cells originating from progenitors previously expressing *Wnt1* are fluorescently tagged with tdT (Wnt1-tdT^{+}). Large Wnt1-$tdT^{+}Plp1^{GFP+}$ fiber–like structures were observed throughout the SAT (Fig. 1A). These structures branched several times until individual Wnt1-$tdT^{+}Plp1^{GFP+}$ cells were observed (Fig. 1B). Wnt1-$tdT^{+}Plp1^{GFP+}$ cells exhibited a predominantly bipolar morphology and formed physical connections end to end, consistent with a Schwann cell identity. In single-cell suspensions of the SAT, 72.6 ± 5.8% of Wnt1-tdT^{+} cells expressed the glial cell marker $Plp1^{GFP}$, which was not present in the Wnt1-tdT^{-} cell population (Fig. 1, C and D). In cross sections of the SAT, large Wnt1-tdT^{+} fibers containing cells were observed to penetrate deep within the adipose and could be observed entering the adipose alone (Fig. 1E) or alongside blood vessels (Fig. 1F). Tau^{GFP};Wnt1::Cre;$ROSA26^{tdTomato}$ (Tau^{GFP};Wnt1-tdT) mice were used to determine coexpression between GFP driven by expression of the neuronal marker *Tau* and cell structures of NC lineage. Wnt1-tdT expression overlapped with Tau^{GFP} in the adipose tissue, confirming that these NC-derived structures were NFBs (Fig. 1F). Within NFBs, Wnt1-tdT^{+} cells and Wnt1-$tdT^{+}Tau^{GFP+}$ nerve fiber processes were observed (Fig. 1G). Only Wnt1-tdT^{+} cells and no Wnt1-$tdT^{+}Tau^{GFP+}$ cells were observed in single-cell suspensions of digested SAT, indicating that Wnt1-$tdT^{+}Tau^{GFP+}$ nerve fibers originate

extrinsically to the SAT. To characterize Schwann cells and nerve fiber processes in the SAT, $Plp1^{GFP}$;BAF53b::Cre;$ROSA26^{tdTomato}$ ($Plp1^{GFP}$;BAF53b-tdT) mice were bred in which GFP is driven by the expression of the glial cell–specific marker *Plp1* and committed neurons are tagged by tdT via Cre recombinase under the control of *Actl6b* (BAF53b). $Plp1^{GFP+}$ cells were confirmed to be closely juxtaposed to BAF53b-tdT^+ nerve fibers, which did not originate from cell bodies within the SAT, and is consistent with a supporting role of $Plp1^{GFP+}$ cells for extrinsic nerve fibers in NFBs (Fig. 1H) and individual nerve fiber processes throughout the SAT (Fig. 1I).

NSCs in the SAT originate from NC-derived Schwann cells

NC-derived (Wnt1-tdT^+) cells from the SAT were isolated from enzymatically digested SAT (Fig. 2A). NFBs from the SAT were resistant to enzymatic digestion and are removed after traditional filtration procedures to produce single-cell suspensions of the SAT (Fig. 2, B and C). Only 0.27 ± 0.09% of nucleated cells from the SAT were Wnt1-tdT^+ (Fig. 2D). When filtered cells, which excludes the NFBs, isolated from the SAT are cultured under low attachment conditions with neuroproliferation medium, spheroids form in vitro, and the proportion of Wnt1-tdT^+ cells increases ~6.5-fold (Fig. 2D). Cells seeded without prior filtration and cultured under the same conditions form spheroids with a ~57.8-fold enrichment of Wnt1-tdT^+ cells, confirming that the majority of NC-derived cells originate from NFBs (Fig. 2D). Individual spheroids were heterogeneous, with Wnt1-tdT^+ cells primarily occupying the center of spheroids (Fig. 2, E and G). Purified Wnt1-tdT^+ cells isolated from heterogeneous spheroids were capable of reforming spheroids and proliferating without the support of Wnt1-tdT^- cells (Fig. 2, F and H).

Previously, it was suggested that the NC gives rise to preadipocytes in the SAT (19). An adipogenesis assay was conducted using purified populations of Wnt1-tdT^+ and Wnt1-tdT^- cells isolated from heterogeneous spheroids (Fig. 2I). The proportion of Oil Red O^+ adipocytes was substantially elevated in Wnt1-tdT^- cultures exposed to adipogenesis induction medium (AM) compared to those containing Wnt1-tdT^+ cells (Fig. 2J). Adipogenesis was not detected in Wnt1-tdT^+ cultures in either culture condition (Fig. 2J). In dissociated spheroids, 96.0 ± 0.2% of Wnt1-tdT^+ cells expressed the glial cell marker $Plp1^{GFP}$, which was not detected in the Wnt1-tdT^- population, indicating enrichment of NC-derived glial cells (Fig. 2K). When the adipogenesis assay was performed using heterogeneous cells, no Wnt1-tdT^+ adipocytes were observed and $Plp1^{GFP}$ was expressed by nearly all Wnt1-tdT^+ cells, indicating that NC-derived cells from the SAT favor a glial phenotype (Fig. 2L). Furthermore, when SAT was digested and cultured using methods intended for MSC isolation, dual Wnt1-tdT^+Plp1^{GFP+} cells were observed to persist in MSC culture media, representing a contaminating cell population (fig. S1). Wnt1-tdT^+ cells were responsive to neural differentiation medium in cultures of the heterogeneous cells from the adipose and were the only cell type to express the neuronal marker TUBB3 (Fig. 2M). Purified cultures of Wnt1-tdT^+ cells formed $TUBB3^+$ neurons and glial fibrillary acidic protein–positive ($GFAP^+$) glial cells in similar conditions, suggesting that Wnt1-tdT^+ cells contain an NSC population (Fig. 2N). Using $Plp1^{GFP}$; BAF53b-tdT glial-neuron reporter mice, expression of $Plp1^{GFP}$ and BAF53b-tdT was observed in SAT NFBs (Fig. 2O); however, $Plp1^{GFP}$ expression was elevated and BAF53b-tdT expression was markedly

reduced during spheroid culture (Fig. 2, O to Q). Production of tdT cannot be muted after Cre-Lox recombination in the Plp1^{GFP};BAF53b-tdT model; therefore, the loss of BAF53b-tdT expression in NFBs can be explained by the initial absence of BAF53b-tdT^{+} neuronal bodies and gradual breakdown of the neuronal fibers from extrinsic sources upon being severed (fig. S2 and movie S1). Analysis by flow cytometry revealed a large number of Plp1^{GFP+} cells with smaller populations of BAF53b-tdT^{+} and dual Plp1^{GFP+} BAF53b-tdT^{+} cells in heterogeneous neurospheres (fig. S3). The presence of BAF53b-tdT^{+} and dual Plp1^{GFP+} BAF53b-tdT^{+} cell populations was validated by in vitro culture on fibronectin. Furthermore, both these cell populations arose from purified Plp1^{GFP+} cells in monolayer cultures (fig. S3). When Plp1^{GFP+} and Plp1^{GFP-} cells were purified and cultured separately in neuronal differentiation conditions, Plp1^{GFP+} cells could give rise to morphologically distinct BAF53b-tdT^{+} neurons with multiple neural processes, but these were not observed in Plp1^{GFP-} cultures (Fig. 2R and fig. S3). Thus, our data suggest that NC-derived Schwann cells are able to give rise to SAT-NSCs.

In vitro culture of Schwann cells induces reprogramming pathways to generate SAT-NSCs

On the basis of our data above, the NC-derived Wnt1-tdT^{+} cells in SAT likely represent Schwann cells. As no neuronal cell bodies are present in the SAT, these Schwann cells appear to acquire their neurogenic potential via reprogramming in vitro. To examine the transition of SAT Schwann cells to SAT-NSCs, we compared their transcriptomes. A total of 329 genes were up-regulated in SAT-NSCs compared with Schwann cells, with an enrichment of genes associated with neurogenesis and nervous system development processes (Fig. 3, A and B). We validated that the NC-derived SAT cells represent Schwann cells by demonstrating their high expression of Schwann cell markers, as shown in Fig. 3C, generated from a published SAT transcriptomic dataset (20). These genes were largely down-regulated after generation of SAT-NSCs, including genes encoding myelin proteins such as *Mpz* (−451-fold), *Pmp22* (−281-fold), *Mal* (−222-fold), and *Mbp* (−197-fold). The loss of Schwann cell properties indicated that SAT-NSCs may be formed via mechanisms of dedifferentiation. This was reinforced by analysis indicating that differentially expressed genes (DEGs) up-regulated in SAT-NSCs are more enriched for embryonic properties (26 of 329, 7.90%) when compared with DEGs up-regulated in Schwann cells (39 of 1121, 3.47%; chi-squared test, $P < 0.001$; Fig. 3D). Further examination identified down-regulation of Schwann cell markers (*Cnp*, −8-fold; *Egr2*, −13-fold; and *S100b*, −5-fold; Fig. 3E) and an up-regulation in neurogenic markers, including *Uchl1* (PGP9.5, 56-fold), *Tubb3* (TUBB3, 5-fold), and *Map2* (3-fold), suggesting that SAT-NSCs are capable of deviating from a Schwann cell restricted fate (Fig. 3E). Furthermore, the expression of several NC stem cell markers was up-regulated, including *Nes* (57-fold), *Ngfr* (P75, 36-fold), and *Sox2* (9-fold; Fig. 3E). These features were consistent with NSCs isolated from the ENS, with 24% of genes up-regulated in SAT-NSCs shared between these cell types (Fig. 3F).

To validate the ability of Schwann cells to acquire stem cell properties, the expression of the NSC marker *Nes* was studied in Nestin^{GFP};Wnt1::Cre;ROSA26^{tdTomato} (Nestin^{GFP};Wnt1-tdT) reporter mice. In the SAT, Wnt1-tdT and Nestin^{GFP} were restricted to separate cell populations in NFBs (Fig. 3G) and the surrounding tissue (Fig. 3H). Likewise, NFBs isolated from the SAT exhibited minimal expression of Nestin^{GFP} (Fig. 3I). After 3 days

in culture, expression of Nestin^{GFP} was induced in the NFBs, which formed spheroids by 10 days and continued to exhibit high Nestin^{GFP} expression, consistent with gene expression data (Figs. 2, E and F, and 3J). Similarly, the expression of the NC-derived NSC marker P75 (NGFR) was confirmed at the protein level in heterogeneous spheroids (Fig. 3K). P75 colocalized with the majority of Wnt1-tdT^{+} cells with minimal expression in the Wnt1-tdT^{-} cells, indicating its high specificity as a SAT-NSC marker (Fig. 3L). In purified neurospheres, expression of GDNF was validated by immunohistochemistry (Fig. 3M). SAT-NSCs expressed the neuronal-glial fate regulation receptor Notch1 and the cell proliferation marker Ki67 in the periphery of the spheres (Fig. 3N).

The gastrointestinal environment supports SAT-NSC engraftment and promotes enteric neuronal differentiation

Considering that NSCs from the NC give rise to enteric neurons in the embryonic environment and Schwann cells can give rise to enteric neurons postnatally (17, 18), we examined the fate of SAT-NSCs in the gut environment in vivo. Neurospheres generated from Wnt1-tdT^{+} cells were implanted into the smooth muscle wall of the colorectum of adult mice (Fig. 4, A and C). All neurospheres generated from purified Wnt1-tdT^{+} cells survived, engrafted, and migrated within the intestinal wall of allogeneic recipients (n = 9/9 mice; Fig. 4D). The area covered by implanted SAT-NSCs increased gradually with time posttransplantation, with a 20.17 ± 6.74–mm^2 coverage area after 8 weeks from single implanted neurospheres (Fig. 4, E to H). In cross sections of the colon, SAT-NSCs were confirmed to engraft into the appropriate layer of the myenteric plexus, between the circular and longitudinal muscle (Fig. 4I), with many transplanted cells expressing the neuronal marker TUBB3 after 8 weeks (Fig. 4J). Similar observations were made in whole-mount preparations of the smooth muscle, confirming that SAT-NSCs are capable of survival and neuronal differentiation within the intermyenteric layer of the gut (Fig. 4K). Transplanted cells formed ganglia-like structures containing neurons (Fig. 4, L and M), as evidenced by their immunoreactivity for TUBB3, neuron-specific enolase (Fig. 4N), and the induction of transgenic Tau^{GFP} expression in SAT-NSCs isolated from Tau^{GFP};Wnt1-tdT mice (Fig. 4O). Transplanted Wnt1-tdT^{+} cells formed physical connections with the host ENS and were incorporated into myenteric ganglia containing both endogenous TUBB3 immunoreactive cells and transplanted Wnt1-tdT^{+} cells (Fig. 4P). Neuronal subtype differentiation consistent with an enteric neuronal phenotype was observed at 8 weeks after transplantation with Wnt1-tdT^{+} cells expressing calretinin (Calr), the vesicular acetylcholine transporter (VAChT), and neuropeptide Y (NPY; Fig. 4, Q to T). Immunoreactivity to Substance P, CGRP, ENK, and TH was not detected in these experiments, suggesting that SAT-NSCs may not recapitulate all enteric neuronal subtypes at the time frames examined (fig. S4).

In similar experiments, SAT-NSC neurospheres from Wnt1-tdT mice survived and thrived after implantation into muscularis propria preparations of the distal colon from wild-type (WT) recipient mice ex vivo. Extensive migration of Wnt1-tdT^{+} cells was observed within the smooth muscle wall (fig. S5A). After 7 days, Wnt1-tdT^{+} transplanted cells were observed to express the enteric neuron marker TUBB3 (fig. S5A) and to integrate with endogenous TUBB3 immunoreactive ganglia of the myenteric plexus (fig. S5B). This was

validated in coculture experiments with mixed cell spheroids from the SAT of Wnt1-tdT mice and the colonic muscularis propria of $Plp1^{GFP}$ mice (fig. S5C). Wnt1-tdT^{+} SAT-NSCs and $Plp1^{GFP+}$ enteric glial cells aggregated into ganglia-like complexes in vitro, and long Wnt1-tdT^{+} fibers were observed to project through enteric $Plp1^{GFP+}$ ganglia, suggesting an affinity between SAT-NSCs and ENS cells (fig. S5, D to F). Evidence of enteric neuronal subtype differentiation was observed in these organ cultures with expression of NOS1 by transplanted SAT-NSCs (Fig. 4U).

SAT-NSC transplantation ameliorates models of neurogastrointestinal disease

We evaluated the therapeutic potential of SAT-NSCs to treat neurogastrointestinal disorders in mouse models of gastroparesis and HSCR. To examine the effects of SAT-NSC transplantation on gastric emptying in a model of gastroparesis, neurospheres were implanted into the stomach wall of $nNOS^{-/-}$ mice (Fig. 5A). Cells were administered via laparotomy and microsurgical implantation of neurospheres into the muscularis externa of the gastric antrum, just proximal to the pylorus (Fig. 5A). SAT-NSCs engrafted in the stomach (Fig. 5B) and had projected nerve fibers (Fig. 5C) at 10 weeks after implantation. SAT-NSC implantation partially reduced the enlarged stomach size of $nNOS^{-/-}$ mice (Fig. 5, D and E). Radiographic gastric emptying assays were performed to assess the effects of SAT-NSCs on the emptying of solid and liquid materials that were gavaged to the stomach (Fig. 5F). SAT-NSC implantation improved gastric emptying of solids compared with naïve and sham-treated nNOS knockout (KO) mice, indicating an amelioration of gastroparesis (Fig. 5G). Similarly, SAT-NSCs ameliorated liquid emptying in nNOS KO mice (Fig. 5H).

Considering the intestinal milieu appears to promote neural differentiation of SAT-NSCs, we evaluated the effects of the differing microenvironments of the colon and stomach on the properties of SAT-NSCs. Neurospheres were transplanted to ex vivo tissue preparations of colon and gastric antrum from the same recipients and were cultured for 7 days to assess migration, proliferation by EdU incorporation, and neural differentiation by immunohistochemistry for TUBB3 (Fig. 5, I and J). The microenvironment of the antrum was preferential toward SAT-NSC spreading (Fig. 5K), with less neuronal differentiation (Fig. 5L) and higher cell proliferation than SAT-NSCs transplanted into the colon (Fig. 5M), which indicates that the properties of SAT-NSCs are dependent on the recipient tissue microenvironment.

To examine the effects of SAT-NSC in a model of HSCR, neurospheres were implanted to the colorectum of $Ednrb^{-/-}$ mice with distal colonic aganglionosis. As demonstrated in the Wnt1-tdT; $Ednrb^{-/-}$ transgenic mouse (Fig. 6A), the Ednrb-null mutation results in intestinal aganglionosis in the midcolon to the rectum with hypertrophic nerve fibers from extrinsic sources present in the aganglionic segment, typical of short-segment human HSCR. SAT-NSC neurospheres were observed to engraft and spread throughout the aganglionic environment without the support of a preexisting ENS 2 to 3 weeks after administration (Fig. 6, B and C). Immunohistochemical labeling of whole-mount tissue preparations indicated that SAT-NSCs differentiated into neurons and resided near hypertrophic nerve fibers in the aganglionic segment (Fig. 6, D and E). SAT-NSCs were observed to migrate between the mucosa and circular muscle, and between the circular and longitudinal muscle layers,

in the aganglionic region (Fig. 6, F and G). These locations represent the typical areas of the submucosal and myenteric plexuses, respectively, in normal ganglionated colon. Likewise, several SAT-NSCs differentiated into neurons in the muscularis (Fig. 6, H and I). Mice were assessed for fecal pellet production over 1 hour before euthanasia. Pellet output was observed in 3/5 Ednrb$^{-/-}$ mice with SAT-NSC transplants compared to 0/5 Ednrb$^{-/-}$ nontransplanted controls. In smooth muscle contraction experiments, colonic tissue collected from Ednrb$^{-/-}$ mice exhibited no response to electric field stimulation (EFS), in stark contrast to WT littermates (Fig. 6, J and K). These contractile properties were restored in the colonic regions of Ednrb$^{-/-}$ mice transplanted with SAT-NSCs (Fig. 6, J and K). Application of tetrodotoxin (TTX) negated EFS-evoked contractile responses in the Ednrb WT and Ednrb$^{-/-}$ mice with SAT-NSC transplants, indicating that these responses were neurally mediated (Fig. 6L).

In ex vivo preparations of ganglionic and aganglionic colon, SAT-NSCs engrafted and exhibited equivalent extent of migration, TUBB3 immunoreactivity, and cell proliferation in both microenvironments (Fig. 6, M to Q). Calcium imaging studies using SAT-NSCs derived from Wnt1::Cre;Polr2a$^{GCaMP5g\text{-}tdTomato}$ (Wnt1-GCaMP5-tdT) mice demonstrated that SAT-NSCs transplanted into the aganglionic environment directly respond to EFS by elevating $[Ca^{2+}]_I$, consistent with functional neurons (Fig. 6R and movie S2). Transplanted cells exhibited a fast increase in calcium influx immediately upon EFS, followed by a biexponential decay consistent with the properties of enteric neurons (Fig. 6S, cells 1 and 2) (21). Likewise, many cells exhibited a delayed Gaussian-like response to EFS similar to secondary responses observed in enteric glia (Fig. 6S, cells 3 and 4) (21). Global calcium responses to EFS occurred in transplanted cells immediately preceding the onset of muscle contraction (Fig. 6T). Given the absence of endogenous neurons in Ednrb$^{-/-}$ distal colon, this suggests that SAT-NSCs are able to mediate muscle contraction in the aganglionic segment. Together, the data in Ednrb$^{-/-}$ and nNOS$^{-/-}$ mice demonstrate the potential benefit of SAT-NSCs for the treatment of neurointestinal disease in both aganglionic and ganglionated environments.

Human SAT NFBs contain NSCs

Our data suggest that the NFBs in mice contain the niche of NSCs in the SAT. Human adipose has both sympathetic and sensory innervation. Nevertheless, recent mapping of the human adipose tissue by single-cell RNA sequencing (RNA-seq) failed to detect any glial cell populations (22). Considering studies isolating cells from the SAT are predominantly filtered to obtain single-cell suspensions, the cell composition of undigested NFBs was examined to determine whether it may contain human SAT-NSCs. Human abdominal SAT specimens (Fig. 7A) were observed to contain NFBs as indicated by CDH19 and TUBB3 immunoreactive fibers in cross sections of the superficial SAT (Fig. 7, B and C). Human SAT was minced, digested, and filtered through a 70-μm strainer. The counter-filtered material was examined under light dissection microscopy, and NFBs were manually selected on the basis of their characteristic striations and “frayed” edges observed at the sites of NFB severance (Fig. 7D). Unlike in mice, high quantities of blood vessels and connective tissue were present in the counter-filtered SAT. Isolation of NFBs was confirmed by immunoreactivity for TUBB3 (Fig. 7E). Nucleated cells were observed juxtaposed to

TUBB3 nerve fibers in whole-mounts (Fig. 7F) of the human SAT NFB. Similar to mice, human SAT NFBs could be cultured in vitro in neuroproliferation medium (Fig. 7G), where they self-remodeled into free-floating spheroid structures, and this was observed for NFBs obtained from all subjects ($n = 3$; Fig. 7H). In SAT processed by enzymatic and mechanical dissociation, nine of nine NFBs formed spheroids, in contrast to only 4 of 18 NFBs obtained from mechanical digestion alone. Spheroids generated from NFBs exhibited a 63.7-fold change ($P < 0.0001$, $n = 3$) in *PLP1* expression compared with those derived from cells of filtered SAT cultured in the same medium ($n = 4$), confirming the successful enrichment of SAT-NSCs from NFBs as observed in mice (fig. S6). Human SAT NFB–derived spheroids were subsequently cultured on a fibronectin-coated surface to promote cell migration. These cells expressed the NC marker P75, which was identified as a specific marker for SAT-NSCs in mice (Fig. 7I), and colocalized with the expression of the NC, NSC, and glial cell marker, SOX10 (Fig. 7J). Low-input RNA-seq was performed on SAT NFB–derived spheroids and spheroids generated from filtered single-cell suspensions of adipose (not containing NFBs) obtained from the same donors and cultured in the same conditions. A total of 2421 DEGs [false discovery rate (FDR), 0.05] were identified between these cells (data files S1 and S2). As shown in Fig. 7K, genes significantly up-regulated in SAT NFB–derived spheroids included key NC stem cell markers such as *NGFR* (594-fold) and *SOX10* (417-fold); neuronal marker *SNAP25* (4.6-fold); neurotrophic factors, *BDNF* (68.8-fold) and *GDNF* (25.7-fold); and *PLP1* (60.1 fold). To identify potential markers of SAT-NSCs, we compared the top 605 up-regulated genes (FDR, 0.01) in this dataset to our previous analysis of mouse SAT-NSCs and Schwann cells (Fig. 3, C to E) and identified 40 shared up-regulated genes in SAT-NSCs from both species (Fig. 7, L to M). This included several markers such as *NGFR* (594-fold), *TMEM59L* (1226.5-fold), *GFRA1* (9.3-fold), and *ITGB8* (23.2-fold). Human SAT NFB–derived spheroids were transplanted ex vivo onto mouse colon, where the cells engrafted, migrated, and expressed TUBB3 after 7 days in culture, consistent with enteric neuronal differentiation (Fig. 7N). These findings confirm that human subcutaneous fat contains a similar population of SAT-NSCs as identified in the mouse, which share similar properties in both species including the expression of comparable markers, such as NGFR (P75) and PLP1; can be isolated from the SAT NFB niche; and have neurogenic potential after neurosphere generation in vitro.

DISCUSSION

In this study, we identify a pool of NSCs residing within a nervous system niche in the SAT of mice and humans. We describe protocols for the efficient isolation and expansion of these cells from NFBs obtained from digested SAT. These SAT-NSCs were found to arise from NC-derived Schwann cells that acquire a neural fate in appropriate in vitro conditions, a process not normally occurring in the endogenous SAT. The cells have the ability to respond to environmental cues, such as those from the gut, which promoted enteric neuronal differentiation and integration into communicating neural networks. SAT-NSCs surgically transplanted to the stomach and colon exhibited remarkable survival, migration, and engraftment within the endogenous ENS, signifying their potential application as a cellular therapy for gastrointestinal disorders of the ENS.

Previous studies have demonstrated the potential of human SAT as a source of NSCs with an unknown origin; however, the cells generated using these protocols are too scarce or impure to perform detailed analysis or transplantation experiments (3). Our data indicate that SAT-NSCs are derived from NC-derived Schwann cells and are contained within the NFBs in mice and humans. This critical insight facilitated the development of the protocols detailed in this study to isolate SAT-NSCs, which might represent a substantial advance in the study of SAT-NSC biology and their therapeutic potential for neural diseases. Human adipose has input from the sympathetic nervous system and sensory innervation. Nevertheless, recent mapping of the human adipose tissue by single-cell RNA-seq failed to detect any glial cell populations (22). Thus, transcriptomic mapping of the human adipose on the single-cell resolution appears to be incomplete. The lack of glial cells in single-cell suspensions may be explained by the cell isolation procedures used. In our study, SAT-derived nerve fibers were poorly digested, which may be attributed to their unique extracellular matrix composition and high lipid content (23). When undigested NFBs are removed to obtain single-cell suspensions, the yields of SAT-NSCs are low. Conversely, large numbers of SAT-NSCs can be generated when using the counter-filtered solution. In standard protocols harvesting adipose-derived cells, the remaining pellet is resuspended and filtered at 40 to 70 μm^2 to obtain a single-cell suspension of the stromal vascular fraction of the adipose tissue (24, 25). Our data show that this common process removes the main pool of SAT-NSCs, and, conversely, counter filtration can be leveraged to obtain enriched SAT-NSC populations from human and mouse SAT.

MSCs from the adipose tissue were first reported to transdifferentiate into neuronal and glial subtypes in 2002 (1). These results, repeated by many groups, were founded on morphological characteristics and transient expression of neural or glial cytoskeletal proteins. The occurrence of neural transdifferentiation of MSCs, however, is debated with neuronal-like morphology and marker expression considered by some as an artifact of several factors such as cytoskeletal filament destabilization after exposure to toxic chemicals or epigenetic instability during long-term in vitro culture (4). These methods of transdifferentiation were deemed suboptimal for the production of functionally competent neurons for therapeutic application (4, 5). Further confounding these studies, some adipose stem cells are found to express neurogenic or gliogenic markers before neuronal induction protocols (26). An alternate hypothesis was formulated to explain the presence of glia and neurons in MSC cultures, which proposed the existence of a rare unidentified cell type that could expand and differentiate in appropriate neural induction conditions (5). Our findings confirm that the SAT contains a resident population of Schwann cells that are present during culture of heterogeneous cells from dissociated adipose tissue. We show that these Schwann cells represent the source of neurons and glial cells as these are not observed in cultures of mesenchymal cells that do not contain NC or glial cell markers, despite being cultured in conditions favoring neurogenesis. This observation supports our finding that NC-derived Schwann cells represent the elusive source of SAT-NSCs. This may also explain why the nerve fiber–rich adipose tissue produces “MSCs” with greater neural and glial differentiation potential than that of the bone marrow (27).

Although the NC gives rise to adipocytes in the cephalic region, reports of this phenomenon in the trunk SAT are conflicting, with one study reporting NC-derived adipocytes are absent

(28) and another suggesting the presence of adipocyte-restricted progenitors derived from the NC (19). In our study, no NC-derived adipocytes were observed in the SAT in vivo, and only $Plp1^{GFP+}$ Schwann cells or Tau^{GFP+} nerve fibers expressed the NC tracer Wnt1-tdT. Similarly, NC-derived cells isolated from the SAT were not capable of differentiation into adipocytes in adipogenic culture conditions, in contrast to non–NC-derived cells, which exhibited robust adipogenesis. During these assays, the NC-derived cells maintained expression of the Schwann cell marker $Plp1^{GFP}$, suggesting that SAT-NSCs may not be capable of ectomesenchymal differentiation.

Considering that there are no neuronal cell bodies in the SAT, the neurogenic potential of SAT-NSCs appears to be physiologically irrelevant. It is therefore intriguing why they retain this multipotency from their stem cell progenitors, the embryonic Schwann cell precursors. One possibility is that all postnatal NFBs contain Schwann cells with the capability to undergo neurogenesis in response to environmental cues. Schwann cells have been observed to transdifferentiate into enteric neurons and glial cells postnatally in mice and zebrafish (17, 18). Another possibility is that SAT-NSCs are not physiologically relevant but rather artificially acquire multipotentiality after dedifferentiation in vitro. Our data indicate that the expression of common NC-derived NSC markers, such as *Nestin*, *Ngfr*, and *Sox2* (29), appears to be acquired, or markedly up-regulated, in Schwann cells of the SAT only after in vitro culture, supporting a process of dedifferentiation. This phenomenon also occurs in oligodendrocyte precursors after neurogenic reprogramming in vitro despite its questionable physiological relevance (30). Likewise, just as mature chondrocytes can dedifferentiate into cells with osteogenic and adipogenic potential in vitro, MSC plasticity may also be an experimental artifact that does not reflect the physiological role of its in vivo progenitors (31, 32).

Alternatively, there is evidence that the Schwann cell dedifferentiation we identified in vitro is similar to physiological responses observed in vivo. Crush injury causes substantial reprogramming of Schwann cells in vivo (16). Considering Schwann cells lose the expression of myelination genes and gain plasticity to differentiate into melanocyte-like cells in vivo, this may be viewed as dedifferentiation to an NC cell progenitor similar to embryonic Schwann cell precursor (33). Notch signaling is critical in Schwann cell demyelination and conversion to an immature phenotype (34). Notch 1 expression was detected in SAT-NSC neurospheres, and therefore, the gain of multipotency in vitro in SAT-NSCs from Schwann cells may reflect these physiological pathways.

The NC gives rise to the ENS, an expansive network of neurons and glial cells in the gastrointestinal tract that regulates essential gut functions, including motility, intestinal secretion, and vasomotor function (35). In our study, SAT-NSCs derived from Schwann cells differentiated into neurons after transplantation to the gut ex vivo and in vivo. Similarly, Schwann cells differentiate into enteric neurons and glial cells postnatally in mice and zebrafish after reaching the intestine (17, 18). NC stem cells from human iPSCs differentiate into enteric neurons when cocultured with gut tissue explants (36). Together, these studies suggest that the gut has a local environmental signaling milieu that assists in enteric neuron differentiation from a variety of endogenous and transplanted progenitor sources. Furthermore, our data indicate that the differing microenvironments of gastrointestinal

regions, but not aganglionosis, have a substantial influence on the migration, proliferation, and differentiation capacity of transplanted NSCs.

Limited treatment options are available for the management of neurointestinal diseases including HSCR and gastroparesis. Surgical removal of the colon is currently the only viable treatment for HSCR, but more than 50% of patients suffer from postoperative complications that include constipation, fecal incontinence, and enterocolitis (37). Similarly, prokinetics and surgical interventions in gastroparesis often fail to reduce symptoms or cause severe side effects in gastroparesis (38). NSC therapy represents a promising strategy to replace missing enteric neurons and restore gastrointestinal function in HSCR and gastroparesis (39). Our group and others have demonstrated the feasibility of NSCs to engraft, migrate, and differentiate to form neuronal networks when transplanted into mice with HSCR (10, 40). In these studies, NSCs have been isolated from surgically removed gut tissue (Gut-NSC) (40) or genetically modified iPSCs (10). Serious concerns remain over the use of iPSCs in humans because of their tumorigenic potential (11). Alternatively, Gut-NSCs appear safe for clinical use because of their limited replicative potential, but their isolation from an autologous source requires surgical resection of a piece of ganglionated bowel (39). Our data indicate that SAT-NSCs offer a potential source of cells for therapeutic applications in ENS disorders such as HSCR or gastroparesis. In our study, SAT-NSCs engrafted and survived remarkably well after allogeneic transplantation to the colon and stomach in vivo, in contrast to cells like MSCs, which are rapidly cleared or fail to integrate with host tissues (41). Transplanted SAT-NSCs demonstrated properties of cell spreading, neuronal differentiation, control of motor activity, and improvement in gastrointestinal function. Transplanted SAT-NSCs expressed the excitatory enteric neuron markers VAChT and CALR, the inhibitory neuronal marker nNOS, and NPY, which, coupled with our organ bath data, indicate successful differentiation into excitatory and inhibitory motor neurons.

The present study has several limitations worth considering. Although we demonstrate that SAT-NSCs isolated from mice exhibit properties consistent with enteric neurons posttransplantation, including immunohistochemical and transgene markers, calcium signaling dynamics, and functional properties, many of these results are yet to be replicated in human samples. From the presented data, human SAT-NSCs share similar properties to those of mice and differentiate into cells expressing neuronal markers after transplantation to the intestinal environment. Nevertheless, methods to assess the functional relevance of these cells are required, including in vivo transplantation in xenogenic models and use of viral delivery tools for calcium imaging and optogenetics. Furthermore, in this study, SAT-NSCs appeared to differentiate into neurons without the full repertoire of neurotransmitters present in the normal ENS. Expressions of CGRP, Substance P, TH, and ENK were not detected by immunohistochemistry. It is unclear whether this was due to experimental methodology or the innate biology of SAT-NSCs. Likewise, because of the redundancy and shared function of several neurotransmitters, it is uncertain whether transplanted cells are required to fully recapitulate the ENS to produce beneficial effects on motility and other gastrointestinal functions. Further studies should elucidate whether SAT-NSCs can differentiate into the full complement of enteric neuronal subclasses such as sensory, intrinsic primary afferent, and interneurons. A useful comparator could include administration of progenitors of the ENS

(ENSCs) to compare specific attributes between endogenous progenitors and SAT-NSCs that may influence their differentiation potential and therapeutic efficacy.

Because adipose stem cells are widely considered to be safe therapeutic agents for humans and autologous SAT is readily accessible, the derivation of SAT-NSCs offers unprecedented potential for therapeutic application in neurological diseases. Future studies should explore the use of SAT-NSCs in other diseases associated with neuropathy or gliopathy. Furthermore, mechanisms of SAT-NSC differentiation require additional elucidation to develop differentiation conditions tailored to producing cells specific to the targeted pathologies for optimal outcomes.

MATERIALS AND METHODS

Study design

This study was designed to assess whether Schwann cells that populate NFBs reside in the SAT and are a source of SAT-NSCs in mice and human samples. Use of human adipose as clinical waste was approved and followed the institutional guidelines of the Massachusetts General Hospital. All study protocols were IRB committee (2020P000153) and IACUC (2009 N000239) approved. For transplantation studies in models of gastrointestinal disease, all mice were age and sex matched, using littermates as controls, with mice selected for treatment at random. Image and functional analysis were performed in a blinded manner.

Mice

Details of all mice used in this study are described in table S1. All mice were purchased from the Jackson Laboratory with the exception of Nestin^{GFP} and Plp1^{GFP} mice that were donated by J. Dietrich, Massachusetts General Hospital (42), and W. Macklin, University of Colorado (43). All mice were housed and bred under specific pathogen–free conditions at the Center for Comparative Medicine animal facility at Massachusetts General Hospital. Experiments were approved by the Massachusetts General Hospital Institutional Animal Care and Use Committee.

SAT nerve fiber and primary cell isolation

Posterior SAT was collected from euthanized mice and immediately minced and incubated with Collagenase XI (1 mg/ml; Sigma-Aldrich) and Dispase (250 μg/ml; Stemcell Technologies) solution for 40 min at 37°C and triturated every 10 min for dissociation. Tissue suspensions were centrifuged at 500*g* for 5 min, and the supernatant was discarded to remove the excess lipid. The solution was resuspended in phosphate-buffered saline (PBS) and filtered through a 40-μm cell strainer (Corning Inc.) to obtain primary single-cell suspensions for analysis by flow cytometry on a BD FACSAria II Cell Sorter (Becton Dickinson). The cell strainers retained SAT NFBs and were overturned and washed with PBS with generate suspensions containing purified NFBs. Suspensions were centrifuged as above and were either fixed in PFA for histology or resuspended in cell culture media for downstream Schwann cell isolation procedures.

SAT-NSC isolation from mice

Cell solutions containing single cells and NFBs generated from the SAT by enzymatic digestion as described above were resuspended in neurobasal medium and either filtered through a 40-μm cell strainer to generate single-cell suspensions as of standard adipose stem cell isolation procedures (25) or left unfiltered to retain the NFBs. Cells were seeded into six-well low-attachment culture dishes at a density of 5×10^5 cells in 2 ml of neuroproliferation medium consisting of Neurocult Mouse Proliferation Supplement (10%, Stemcell Technologies), basic fibroblast growth factor (20 ng/ml; Stemcell Technologies), epidermal growth factor (20 ng/ml; Stemcell Technologies), heparin (0.0002%; Stemcell Technologies), and penicillin and streptomycin (1%; Life Technologies, Thermo Fisher Scientific) in Neurocult Mouse Basal Medium (Stemcell Technologies). Cells were cultured in a humidified incubator with 5% CO_2, atmospheric oxygen at 37°C. Low media volumes were used to assist with initial cell aggregation. An additional 2 ml of media was added after 3 days, and cells were cultured for 10 days at which point numerous spheroids were observed.

Spheroid-containing solutions were transferred to fibronectin-coated (1:500 of sterile PBS for 2 hours at 37°C) cell culture flasks seeded (7 to 7.5 cm^2/ml of cell solution) and supplemented with 5% fetal bovine serum (FBS) to promote attachment and cell migration from spheroids. After 48 hours, cells were washed with PBS and trypsinized with TryplE Select Enzyme (Life Technologies) for 5 min at 37°C. Trypsinization was neutralized with 1:2 volume of basal media containing 2.5% FBS, and cells were pelleted via centrifugation as described above. Cells were resuspended in neuroproliferation medium and stained with DAPI (4′,6-diamidino-2-phenylindole; 1:1000) for fluorescence-activated cell sorting (FACS) of either Wnt1-tdT− or $Plp1^{GFP}$-expressing cells from transgenic reporter mice. Flow cytometry data were analyzed and presented using FlowJo software (FlowJo). Purified cells obtained via FACS were plated at a density of 1000 cells/cm^2 in 24-well low-attachment plates in culture conditions and media as described above to generate homogeneous neurospheres containing SAT-NSCs.

NFB isolation and culture from human abdominal SAT

Human abdominal SAT was stored overnight at 4°C, cut into ~1-cm^2 pieces, and washed three times in sterile PBS. For enzymatic digestion, pieces of SAT were digested in Liberase Thermolysin High formulation (25 μg/ml; Roche) and Dispase (0.05 U/ml; StemCell Technologies) for 3 hours in a humidified incubator at 37°C. Digested SAT was aliquoted into C-tubes (Miltenyi Biotec) for homogenization using the GentleMACs (program: spleen 1, Miltenyi Biotec) tissue dissociator system (enzymatic and mechanical digestion). In addition, a second method using only mechanical digestion as detailed above without prior incubation in the enzymatic cocktail was performed. The dissociated SAT was filtered through a 70-μm cell strainer, and the counter-filtered material was collected and washed with sterile PBS. Under a light dissection microscope, NFBs were manually collected on the basis of morphology, with NFBs exhibiting characteristic striations and frayed edges observed at the sites where the NFBs had been severed.

NFBs were cut into 1- to 2-mm-long pieces and placed into low-attachment culture dishes (24-well) containing 1 ml of human neural proliferation medium [basic fibroblast growth factor (20 ng/ml; Stemcell Technologies), epidermal growth factor (20 ng/ml; Stemcell Technologies), heparin (0.0002%; Stemcell Technologies), GlutaMAX (1%; Life Technologies), B27 supplement (1%), Primocin (1%), Metronidazole (50 μg/ml), and FBS (5%) in Dulbecco's modified Eagle's medium: Nutrient Mixture F-12 (Gibco, Life Technologies)]. After 3 days, the medium was doubled, and by day 7, NFBs isolated by enzymatic and mechanical digestion had remodeled into spheroids.

After 10 days of culture, spheroids were transferred to tissue culture–treated six-well plates coated with fibronectin with additional media added at a ratio of 2:3. After 2 weeks, cells from the NFB-derived spheroids had migrated onto the surface of the cell culture flask. Cells were trypsinized as described above yielding between 1.5×10^4 to 8.5×10^4 cells per spheroid and were passaged and expanded by replating in 24-well low-attachment tissue culture plates at density of 2.5×10^3 cells/cm^2 in human neuroproliferation medium with weekly replacement of half of the media over 4 weeks.

Statistical analysis

Data analysis was performed using GraphPad Prism v7 (GraphPad Software Inc.). Two-tailed *t* test was performed for all pairwise comparisons. For multiple comparisons, a one-way analysis of variance (ANOVA) was performed with Holm-Sidak test for post hoc analysis on all data unless stated otherwise. Posttest for linear trend was performed on in vivo cell engraftment and migration data (Fig. 4D). For data with nonequal variances, one-way ANOVA was performed with Welch's corrections and Welch's *t* test for post hoc comparisons (Fig. 5, F and G). Nonparametric data were analyzed by Kruskal-Wallis nonparametric ANOVA with Dunn's multiple comparisons test (Fig. 6, H and H′). For all analyses, $P < 0.05$ was considered significant. All data were presented as means ± SEM, unless otherwise stated.

Supplementary Material

Refer to Web version on PubMed Central for supplementary material.

Acknowledgments:

We would like to acknowledge M. McCormack from the Department of Surgery, Plastic Surgery New Innovations Research, MGH for organizing human material for this study, and the laboratory of X. Ai, MGH, for providing reagents.

Funding:

National Institutes of Health grants R01DK119210 to A.M.G., R01DK103785 to A.M.G., R21HD106036 to R.S. and A.M.G., R03HD100762 to R.H., and F32DK121440 to R.A.G.

Data and materials availability:

All data to support the conclusions of this study are present in the main text, Supplementary Materials, or provided within the National Center for Biotechnology Information (NCBI) Gene Expression Omnibus (GEO) repository under the accession GSE200689.

REFERENCES AND NOTES

1. Zuk PA, Zhu M, Ashjian P, De Ugarte DA, Huang JI, Mizuno H, Alfonso ZC, Fraser JK, Benhaim P, Hedrick MH, Human adipose tissue is a source of multipotent stem cells. Mol. Biol. Cell 13, 4279–4295 (2002). [PubMed: 12475952]
2. Chu D-T, Phuong TNT, Tien NLB, Tran DK, Minh LB, Thanh VV, Anh PG, Pham VH, Nga VT, Adipose tissue stem cells for therapy: An update on the progress of isolation, culture, storage, and clinical application. J. Clin. Med. 8, 917 (2019). [PubMed: 31247996]
3. Peng C, Lu L, Li Y, Hu J, Neurospheres induced from human adipose-derived stem cells as a new source of neural progenitor cells. Cell Transplant. 28, 66S–75S (2019). [PubMed: 31813268]
4. Phinney DG, Prockop DJ, Concise review: Mesenchymal stem/multipotent stromal cells: The state of transdifferentiation and modes of tissue repair—Current views. Stem Cells 25, 2896–2902 (2007). [PubMed: 17901396]
5. Krabbe C, Zimmer J, Meyer M, Neural transdifferentiation of mesenchymal stem cells–A critical review. APMIS 113, 831–844 (2005). [PubMed: 16480453]
6. Croft AP, Przyborski SA, Formation of neurons by non-neural adult stem cells: Potential mechanism implicates an artifact of growth in culture. Stem Cells 24, 1841–1851 (2006). [PubMed: 16868208]
7. Lu P, Blesch A, Tuszynski MH, Induction of bone marrow stromal cells to neurons: Differentiation, transdifferentiation, or artifact? J. Neurosci. Res. 77, 174–191 (2004). [PubMed: 15211585]
8. Hotta R, Stamp LA, Foong JP, McConnell SN, Bergner AJ, Anderson RB, Enomoto H, Newgreen DF, Obermayr F, Furness JB, Young HM, Transplanted progenitors generate functional enteric neurons in the postnatal colon. J. Clin. Invest. 123, 1182–1191 (2013). [PubMed: 23454768]
9. Vescovi AL, Parati EA, Gritti A, Poulin P, Ferrario M, Wanke E, Frölichsthal-Schoeller P, Cova L, Arcellana-Panlilio M, Colombo A, Isolation and cloning of multipotential stem cells from the embryonic human CNS and establishment of transplantable human neural stem cell lines by epigenetic stimulation. Exp. Neurol. 156, 71–83 (1999). [PubMed: 10192778]
10. Fattahi F, Steinbeck JA, Kriks S, Tchieu J, Zimmer B, Kishinevsky S, Zeltner N, Mica Y, El-Nachef W, Zhao H, de Stanchina E, Gershon MD, Grikscheit TC, Chen S, Studer L, Deriving human ENS lineages for cell therapy and drug discovery in Hirschsprung disease. Nature 531, 105–109 (2016). [PubMed: 26863197]
11. Deng J, Zhang Y, Xie Y, Zhang L, Tang P, Cell transplantation for spinal cord injury: Tumorigenicity of induced pluripotent stem cell-derived neural stem/progenitor cells. Stem Cells Int. 2018, 5653787 (2018). [PubMed: 29535771]
12. Townsend KL, The re-emergence of adipose innervation as a research focus. Nat. Rev. Endocrinol. 16, 127–128 (2020). [PubMed: 31980753]
13. Furlan A, Adameyko I, Schwann cell precursor: A neural crest cell in disguise? Dev. Biol. 444, S25–S35 (2018). [PubMed: 29454705]
14. Kameneva P, Kastriti ME, Adameyko I, Neuronal lineages derived from the nerve-associated Schwann cell precursors. Cell. Mol. Life Sci. 78, 513–529 (2020). [PubMed: 32748156]
15. Masaki T, Qu J, Cholewa-Waclaw J, Burr K, Raaum R, Rambukkana A, Reprogramming adult Schwann cells to stem cell-like cells by leprosy bacilli promotes dissemination of infection. Cell 152, 51–67 (2013). [PubMed: 23332746]
16. Jessen KR, Mirsky R, The repair Schwann cell and its function in regenerating nerves. J. Physiol. 594, 3521–3531 (2016). [PubMed: 26864683]
17. Uesaka T, Nagashimada M, Enomoto H, Neuronal differentiation in Schwann cell lineage underlies postnatal neurogenesis in the enteric nervous system. J. Neurosci. 35, 9879–9888 (2015). [PubMed: 26156989]
18. El-Nachef WN, Bronner ME, *De novo* enteric neurogenesis in post-embryonic zebrafish from Schwann cell precursors rather than resident cell types. Development 147, dev186619 (2020). [PubMed: 32541008]
19. Sowa Y, Imura T, Numajiri T, Takeda K, Mabuchi Y, Matsuzaki Y, Nishino K, Adipose stromal cells contain phenotypically distinct adipogenic progenitors derived from neural crest. PLOS ONE 8, e84206 (2013). [PubMed: 24391913]

20. Rajbhandari P, Arneson D, Hart SK, Ahn IS, Diamante G, Santos LC, Zaghari N, Feng A-C, Thomas BJ, Vergnes L, Single cell analysis reveals immune cell–adipocyte crosstalk regulating the transcription of thermogenic adipocytes. eLife 8, e49501 (2019). [PubMed: 31644425]
21. Boesmans W, Martens MA, Weltens N, Hao MM, Tack J, Cirillo C, Vanden Berghe P, Imaging neuron-glia interactions in the enteric nervous system. Front. Cell. Neurosci. 7, 183 (2013). [PubMed: 24155689]
22. Vijay J, Gauthier M-F, Biswell RL, Louiselle DA, Johnston JJ, Cheung WA, Belden B, Pramatarova A, Biertho L, Gibson M, Single-cell analysis of human adipose tissue identifies depot- and disease-specific cell types. Nat. Metab. 2, 97–109 (2020). [PubMed: 32066997]
23. Marangon D, Boccazzi M, Lecca D, Fumagalli M, Regulation of oligodendrocyte functions: Targeting lipid metabolism and extracellular matrix for myelin repair. J. Clin. Med. 9, 470 (2020). [PubMed: 32046349]
24. Jang Y, Koh YG, Choi YJ, Kim SH, Yoon DS, Lee M, Lee JW, Characterization of adipose tissue-derived stromal vascular fraction for clinical application to cartilage regeneration. In Vitro Cell. Dev. Biol. Anim. 51, 142–150 (2015). [PubMed: 25361717]
25. Stavely R, Robinson AM, Miller S, Boyd R, Sakkal S, Nurgali K, Allogeneic guinea pig mesenchymal stem cells ameliorate neurological changes in experimental colitis. Stem Cell Res. Ther. 6, 263 (2015). [PubMed: 26718461]
26. Blecker D, Elashry M, Heimann M, Wenisch S, Arnhold S, New insights into the neural differentiation potential of canine adipose tissue-derived mesenchymal stem cells. Anat. Histol. Embryol. 46, 304–315 (2017). [PubMed: 28401575]
27. Zhang H-T, Liu Z-L, Yao X-Q, Yang Z-J, Xu R-X, Neural differentiation ability of mesenchymal stromal cells from bone marrow and adipose tissue: A comparative study. Cytotherapy 14, 1203–1214 (2012). [PubMed: 22909277]
28. Billon N, Iannarelli P, Monteiro MC, Glavieux-Pardanaud C, Richardson WD, Kessaris N, Dani C, Dupin E, The generation of adipocytes by the neural crest. Development 134, 2283–2292 (2007). [PubMed: 17507398]
29. Motohashi T, Kunisada T, Extended multipotency of neural crest cells and neural crest-derived cells. Curr. Top. Dev. Biol. 111, 69–95 (2015). [PubMed: 25662258]
30. Kondo T, Raff M, Oligodendrocyte precursor cells reprogrammed to become multipotential CNS stem cells. Science 289, 1754–1757 (2000). [PubMed: 10976069]
31. Barbero A, Ploegert S, Heberer M, Martin I, Plasticity of clonal populations of dedifferentiated adult human articular chondrocytes. Arthritis Rheum. 48, 1315–1325 (2003). [PubMed: 12746904]
32. da Silva Meirelles L, Caplan AI, Nardi NB, In search of the in vivo identity of mesenchymal stem cells. Stem Cells 26, 2287–2299 (2008). [PubMed: 18566331]
33. Rizvi TA, Huang Y, Sidani A, Atit R, Largaespada DA, Boissy RE, Ratner N, A novel cytokine pathway suppresses glial cell melanogenesis after injury to adult nerve. J. Neurosci. 22, 9831–9840 (2002). [PubMed: 12427839]
34. Jessen KR, Mirsky R, Negative regulation of myelination: Relevance for development, injury, and demyelinating disease. Glia 56, 1552–1565 (2008). [PubMed: 18803323]
35. Furness JB, The enteric nervous system and neurogastroenterology. Nat. Rev. Gastroenterol. Hepatol. 9, 286–294 (2012). [PubMed: 22392290]
36. Li W, Huang L, Zeng J, Lin W, Li K, Sun J, Huang W, Chen J, Wang G, Ke Q, Duan J, Lai X, Chen R, Liu M, Liu Y, Wang T, Yang X, Chen Y, Xia H, Xiang AP, Characterization and transplantation of enteric neural crest cells from human induced pluripotent stem cells. Mol. Psychiatry 23, 499–508 (2018). [PubMed: 27777423]
37. Catto-Smith AG, Trajanovska M, Taylor RG, Long-term continence after surgery for Hirschsprung's disease. J. Gastroenterol. Hepatol. 22, 2273–2282 (2007). [PubMed: 18031392]
38. Myint AS, Rieders B, Tashkandi M, Borum ML, Koh JM, Stephen S, Doman DB, Current and emerging therapeutic options for gastroparesis. Gastroenterol. Hepatol. 14, 639–645 (2018).
39. Burns AJ, Goldstein AM, Newgreen DF, Stamp L, Schafer KH, Metzger M, Hotta R, Young HM, Andrews PW, Thapar N, Belkind-Gerson J, Bondurand N, Bornstein JC, Chan WY, Cheah K, Gershon MD, Heuckeroth RO, Hofstra RM, Just L, Kapur RP, King SK, McCann CJ, Nagy N, Ngan E, Obermayr F, Pachnis V, Pasricha PJ, Sham MH, Tam P, Vanden Berghe P, White paper on

guidelines concerning enteric nervous system stem cell therapy for enteric neuropathies. Dev. Biol. 417, 229–251 (2016). [PubMed: 27059883]

40. Hotta R, Cheng LS, Graham HK, Pan W, Nagy N, Belkind-Gerson J, Goldstein AM, Isogenic enteric neural progenitor cells can replace missing neurons and glia in mice with Hirschsprung disease. Neurogastroenterol. Motil. 28, 498–512 (2016). [PubMed: 26685978]
41. von Bahr L, Batsis I, Moll G, Hägg M, Szakos A, Sundberg B, Uzunel M, Ringden O, Le Blanc K, Analysis of tissues following mesenchymal stromal cell therapy in humans indicates limited long-term engraftment and no ectopic tissue formation. Stem Cells 30, 1575–1578 (2012). [PubMed: 22553154]
42. Mignone JL, Kukekov V, Chiang A-S, Steindler D, Enikolopov G, Neural stem and progenitor cells in nestin-GFP transgenic mice. J. Comp. Neurol. 469, 311–324 (2004). [PubMed: 14730584]
43. Mallon BS, Shick HE, Kidd GJ, Macklin WB, Proteolipid promoter activity distinguishes two populations of NG2-positive cells throughout neonatal cortical development. J. Neurosci. 22, 876–885 (2002). [PubMed: 11826117]
44. Stavely R, Bhave S, Ho WLN, Ahmed M, Pan W, Rahman AA, Ulloa J, Bousquet N, Omer M, Guyer R, Enteric mesenchymal cells support the growth of postnatal enteric neural stem cells. Stem Cells 39, 1236–1252 (2021). [PubMed: 33938072]
45. Stavely R, Robinson AM, Miller S, Boyd R, Sakkal S, Nurgali K, Human adult stem cells derived from adipose tissue and bone marrow attenuate enteric neuropathy in the guinea-pig model of acute colitis. Stem Cell Res. Ther. 6, 244 (2015). [PubMed: 26652292]
46. Nagy N, Barad C, Hotta R, Bhave S, Arciero E, Dora D, Goldstein AM, Collagen 18 and agrin are secreted by neural crest cells to remodel their microenvironment and regulate their migration during enteric nervous system development. Development 145, dev160317 (2018). [PubMed: 29678817]
47. Robinson AM, Rahman AA, Carbone SE, Randall-Demllo S, Filippone R, Bornstein JC, Eri R, Nurgali K, Alterations of colonic function in the Winnie mouse model of spontaneous chronic colitis. Am. J. Physiol.Gastrointest. Liver Physiol. 312, G85–G102 (2017). [PubMed: 27881401]
48. Baker C, Ahmed M, Cheng K, Arciero E, Bhave S, Ho WLN, Goldstein AM, Hotta R, Hypoganglionosis in the gastric antrum causes delayed gastric emptying. Neurogastroenterol. Motil. 32, e13766 (2020). [PubMed: 31773831]
49. Liao Y, Smyth GK, Shi W, FeatureCounts: An efficient general purpose program for assigning sequence reads to genomic features. Bioinformatics 30, 923–930 (2014). [PubMed: 24227677]
50. Robinson MD, McCarthy DJ, Smyth GK, edgeR: A Bioconductor package for differential expression analysis of digital gene expression data. Bioinformatics 26, 139–140 (2010). [PubMed: 19910308]
51. Tarazona S, García F, Ferrer A, Dopazo J, Conesa A, NOIseq: A RNA-seq differential expression method robust for sequencing depth biases. EMBnet J. 17, 18 (2012).
52. Dennis G, Sherman BT, Hosack DA, Yang J, Gao W, Lane HC, Lempicki RA, DAVID: Database for annotation, visualization, and integrated discovery. Genome Biol. 4, R60 (2003).
53. Huang DW, Sherman BT, Lempicki RA, Systematic and integrative analysis of large gene lists using DAVID bioinformatics resources. Nat. Protoc. 4, 44–57 (2008).
54. Huang DW, Sherman BT, Lempicki RA, Bioinformatics enrichment tools: Paths toward the comprehensive functional analysis of large gene lists. Nucleic Acids Res. 37, 1–13 (2008). [PubMed: 19033363]
55. Bhave S, Arciero E, Baker C, Ho WL, Stavely R, Goldstein AM, Hotta R, Enteric neuronal cell therapy reverses architectural changes in a novel diphtheria toxin-mediated model of colonic aganglionosis. Sci. Rep. 9, 18756 (2019). [PubMed: 31822721]
56. Zhan X, Cao M, Yoo AS, Zhang Z, Chen L, Crabtree GR, Wu JI, Generation of BAF53b-Cre transgenic mice with pan-neuronal Cre activities. Genesis 53, 440–448 (2015). [PubMed: 26077106]
57. Hennig GW, Gould TW, Koh SD, Corrigan RD, Heredia DJ, Shonnard MC, Smith TK, Use of genetically encoded calcium indicators (GECIs) combined with advanced motion tracking techniques to examine the behavior of neurons and glia in the enteric nervous system of the intact murine colon. Front. Cell. Neurosci. 9, 436 (2015). [PubMed: 26617487]

58. McClain JL, Gulbransen BD, The acute inhibition of enteric glial metabolism with fluoroacetate alters calcium signaling, hemichannel function, and the expression of key proteins. J. Neurophysiol. 117, 365–375 (2017). [PubMed: 27784805]

59. Mashimo H, Kjellin A, Goyal RK, Gastric stasis in neuronal nitric oxide synthase–Deficient knockout mice. Gastroenterology 119, 766–773 (2000). [PubMed: 10982771]

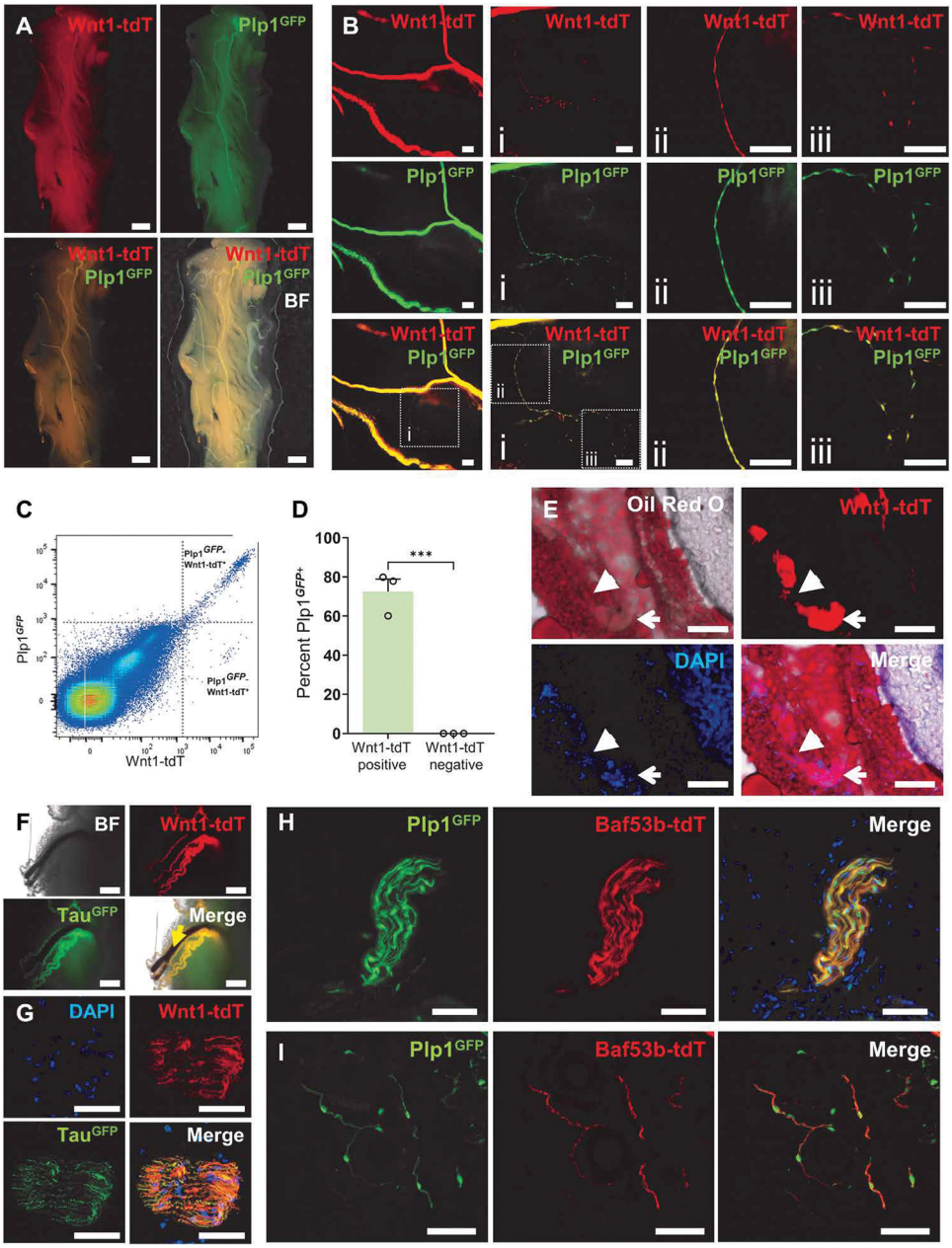

Fig. 1. Characterization of nerve fibers and Schwann cells in the mouse subcutaneous adipose tissue.

Representative low- (**A**) and high-magnification (**B**) images of whole-mount preparations of subcutaneous adipose tissue (SAT) from $Plp1^{GFP}$;Wnt1-tdT mice. Scale bars, 1 mm (A), 200 μm (B), and 100 μm (Bi to Biii). (**C**) Representative dot plots of Wnt1-tdT and $Plp1^{GFP}$ expression in cells from digested SAT. (**D**) Quantification of the percentage of $Plp1^{GFP}$-expressing cells within Wnt1-tdT^{+} and Wnt1-tdT^{-} populations. $n = 3$ mice per group, unpaired t test, $^{***}P < 0.001$. (**E**) Oil Red O staining of lipids in cross sections of the SAT from Wnt-tdT mice. Open arrows indicate nerve fiber bundles (NFBs), and closed arrows denote NFB penetrating into the SAT. Scale bars, 100 μm. Representative images from Tau^{GFP};Wnt1-tdT mice of whole-mount SAT with penetrating blood vessels

(yellow arrow) (**F**) and cross sections of NFBs (**G**). Scale bars, 500 μm (F) and 50 μm (G). Representative images of NFBs (**H**) and individual nerve fiber processes (**I**) in cross sections of SAT from $Plp1^{GFP}$;BAF53b-tdT mice. Scale bars, 50 μm.

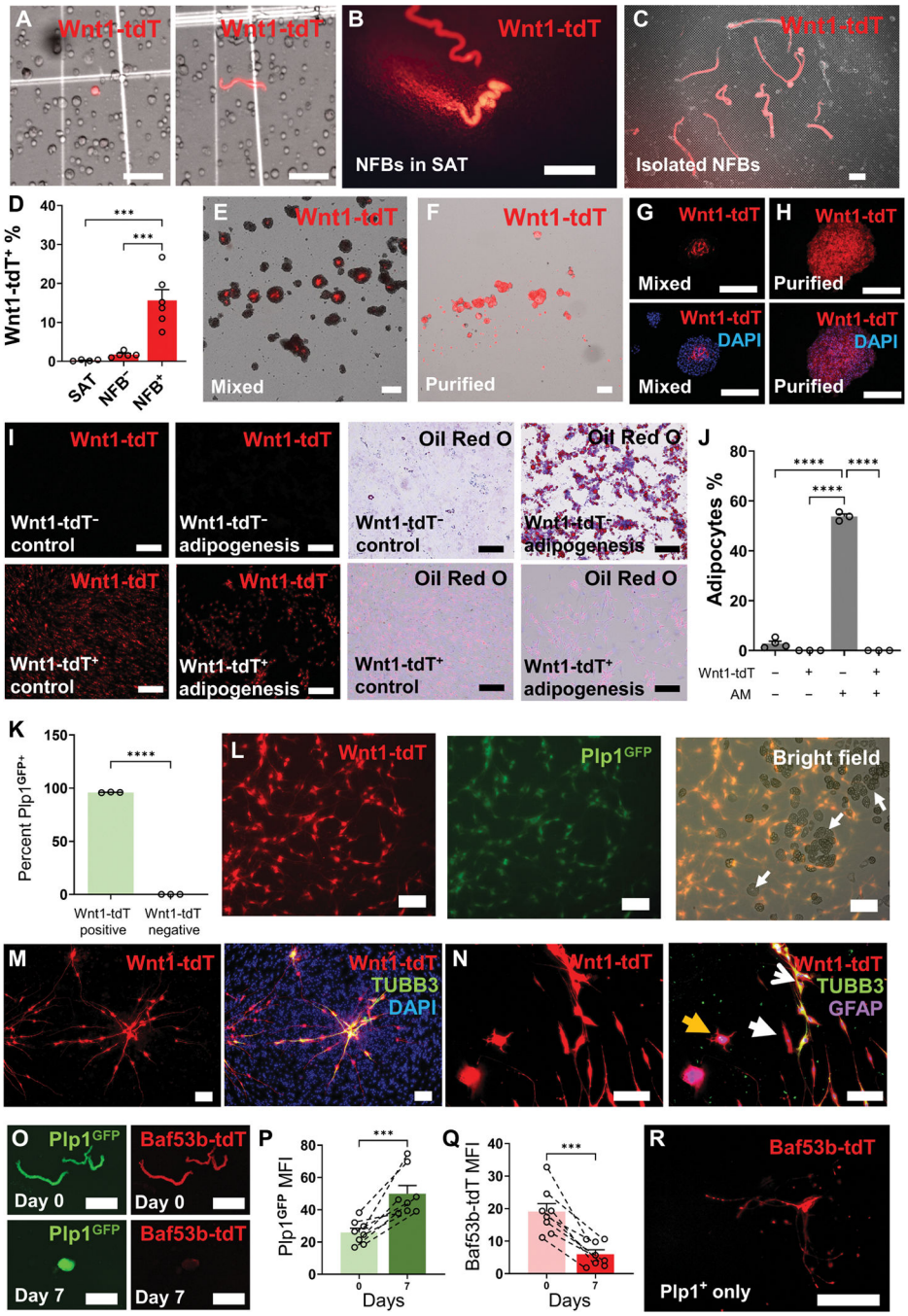

Fig. 2. SAT-NSCs originate from the NFBs of SAT in mice.

(**A**) Representative images of digested cells from the SAT of Wnt1-tdT reporter mice with Wnt1-tdT$^+$ cells displaying spherical (left) and bipolar morphology (right). Scale bars, 50 μm. NFBs from Wnt1-tdT mice visualized in whole-mount SAT (**B**) and after enzymatic digestion of the SAT on a 40-μm cell strainer (**C**). Scale bars, 1 mm. (**D**) Percentage of Wnt1-tdT$^+$ cells within filtered digested SAT (SAT) and cultured SAT-derived spheroids from filtered SAT without NFBs (NFB$^-$) and unfiltered SAT containing NFBs (NFB$^+$). SAT, $n = 4$; NFB$^-$, $n = 5$; and NFB$^+$, $n = 6$ mice per group, one-way ANOVA with Holm-

Sidak multiple comparisons test, ***$P < 0.001$. Representative images of heterogeneous SAT-derived spheroids (Mixed) (**E**) and spheroids cultured from purified Wnt1-tdT$^+$ cells (Purified) (**F**) under free-floating culture conditions. Scale bars, 200 μm (E) and 200 μm (F). (**G** and **H**) Wnt1-tdT expression in cross sections of mixed SAT-derived spheroids (G) and spheroids generated from purified Wnt1-tdT$^+$ cells (H). Scale bars, 200 μm. (**I**) Representative images of adipogenesis assay using Wnt1-tdT$^-$ cells (top row) and Wnt1-tdT$^+$ cells (bottom row) cultured in control or adipogenesis induction medium and stained for lipid vacuoles with Oil Red O. Scale bars, 200 μm. (**J**) Quantitative analysis of Oil Red O–positive adipocytes from Wnt1-tdT$^+$ or Wnt1-tdT$^-$ cells cultured in adipogenesis medium (AM). One-way ANOVA with Holm-Sidak multiple comparisons test, ****$P < 0.0001$. (**K**) Quantification of the percentage of Plp1^{GFP}-expressing cells within Wnt1-tdT$^+$ and Wnt1-tdT$^-$ populations by flow cytometry. $n = 3$ mice per group, unpaired t test, ****$P < 0.0001$. (**L**) Representative images of adipogenesis assay conducted using heterogeneous cells from mixed SAT spheroids expressing Wnt1-tdT (left) Plp1^{GFP} (middle) and bright-field images of adipocytes (right, white arrows). Scale bars, 200 μm. (**M**) Expression of Wnt1-tdT (left) and TUBB3 (right) in heterogeneous cultures from the adipose after neural differentiation. Scale bars, 200 μm. (**N**) Images of Wnt1-tdT expression (left) with immunohistochemistry for GFAP and TUBB3 (right) and merged images after differentiation. Arrows indicate TUBB3$^+$ neurons (open white arrow), GFAP$^+$ glial cells (yellow closed arrow), and cells expressing neither marker (white closed arrow). Scale bars, 200 μm. (**O**) Images of BAF53b-tdT and Plp1^{GFP} expression in isolated NFBs from SAT (day 0) and SAT-NSC neurospheres during culture (day 7). Scale barss, 500 μm. Quantification of the mean fluorescence intensity (MFI) of PLP1^{GFP} (**P**) and BAF53b-tdT (**Q**) in cultured NFBs. n = 8 NFBs per group, paired t test, ***$P < 0.001$. (**R**) Induction of BAF53b-tdT expression from Plp1^{GFP} cells purified from SAT-derived spheroids. Scale bar, 250 μm.

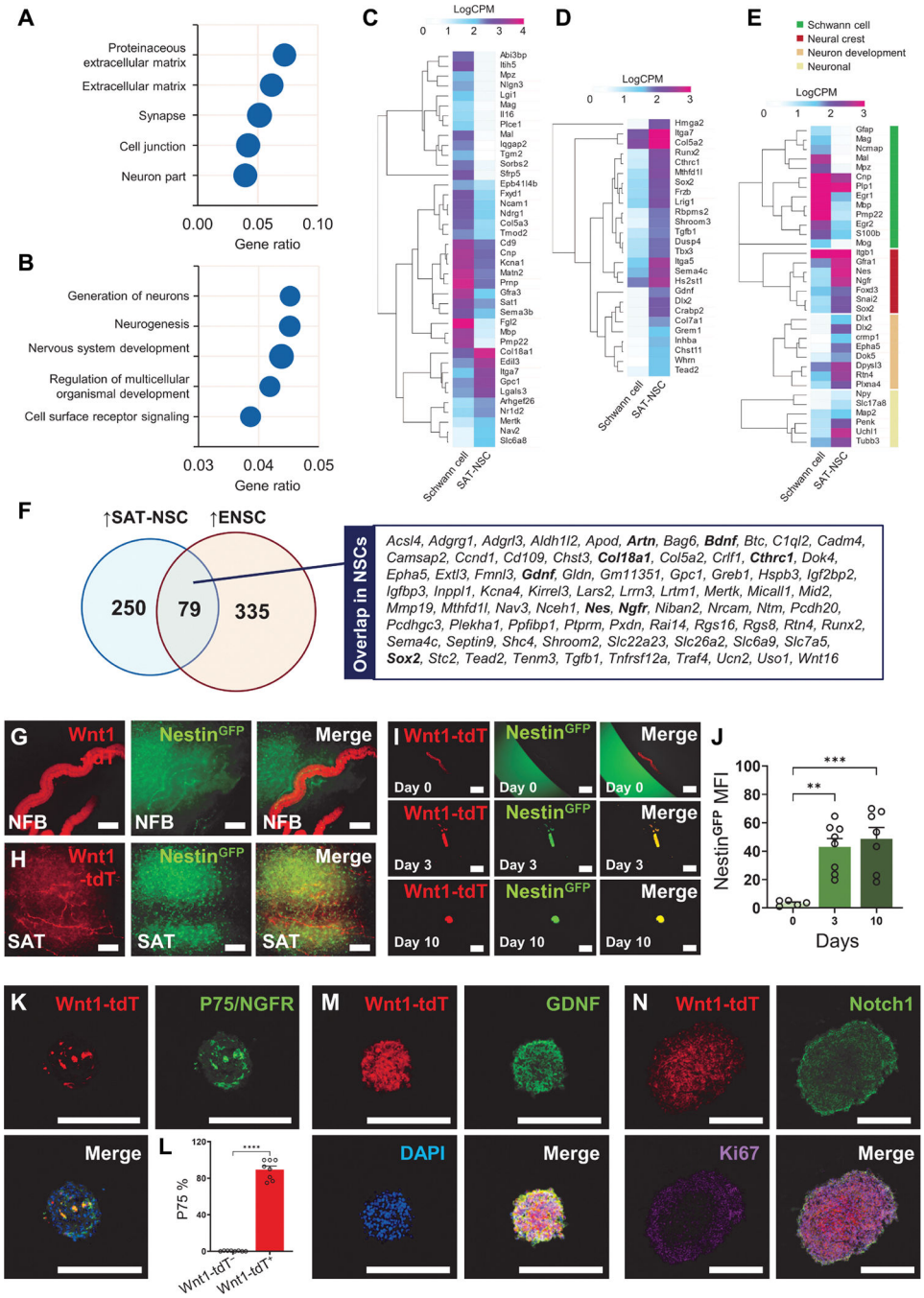

Fig. 3. Neural crest–derived Schwann cells from SAT acquire NSC properties in vitro.

Overrepresentation analysis of cellular components (**A**) and biological processes (**B**) for genes up-regulated in neurospheres generated from Wnt1-tdT^{+} cells compared with Wnt1-tdT^{+} cells obtained from primary SAT. (**C** to **E**) Heatmap representation of Schwann cell markers (C), Embryonic morphogenesis (D), as well as curated Schwann cell, neural crest stem cell, and neuronal genes (E) in Wnt1-tdT^{+} cells from SAT and cultured neurospheres (SAT-NSCs) visualized as LogCPM values. (**F**) Venn diagram of up-regulated DEGs common between SAT-NSCs and enteric neural stem cells (ENSCs). (**G** and **H**) Expression

of Wnt1-tdT and Nestin^{GFP} in the NFB (G) and dispersed Wnt1-tdT^{+} Schwann cells (H) in the SAT. Scale bars, 200 μm. (**I**) NFBs from the digested SAT of Nestin^{GFP}; Wnt1-tdT cultured into spheroids over 10 days in free floating conditions. Scale bars, 500 μm. (**J**) Quantification of the MFI of Nestin^{GFP} in cultured NFBs. Day 0, n = 5; day 3, n = 8; day 10; n = 7 NFBs per group, one-way ANOVA with Holm-Sidak multiple comparisons test, $^{**}P < 0.01$ and $^{***}P < 0.001$. (**K**) Representative images of Wnt1-tdT expression, immunoreactivity for P75/NGFR, and merged image with DAPI of heterogeneous SAT-derived spheroids. Scale bars, 200 μm. (**L**) Quantification of the percentage of P75-expressing cells in the Wnt1-tdT^{+} and Wnt1-tdT^{-} populations of SAT-derived spheroids. n = 8 spheroids, unpaired t test, $^{****}P < 0.0001$. Representative images of Wnt1-tdT expression and immunohistochemistry for GDNF (**M**), Notch1, and Ki67 (**N**) in neurospheres generated from purified Wnt1-tdT^{+} cells. Scale bars, 200 μm.

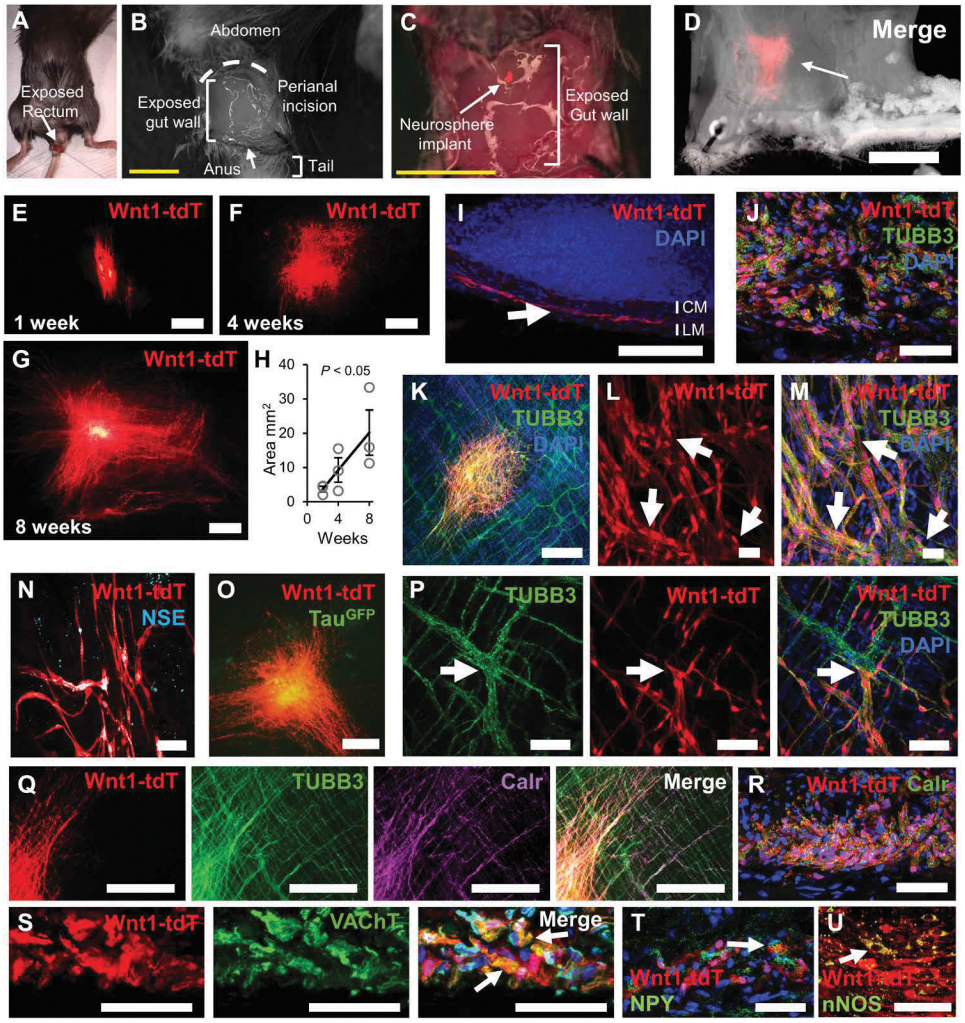

Fig. 4. The gut signaling milieu promotes the enteric differentiation of SAT-NSCs.

Procedure to access the colorectum (**A**) via perianal incision (**B**) and neurosphere implantation to the exposed gut wall (**C**). Scale bars, 5 mm. (**D**) Representative image of bright-field microscopy and Wnt1-tdT expression of transplanted SAT-NSCs. Scale bar, 5 mm. Representative images of transplanted Wnt1-tdT$^+$ SAT-NSCs at 2 (**E**), 4 (**F**), and 8 weeks (**G**) after implantation. Scale bars, 1 mm. (**H**) Quantification of the area occupied by transplanted Wnt1-tdT$^+$ cells over 8 weeks. $n = 3$ mice per group, one-way ANOVA with posttest for linear trend. (**I**) Cross section of the transplanted colon stained with DAPI. Arrow indicated transplanted Wnt1-tdT$^+$ cells located between the circular muscle (CM) and longitudinal muscle (LM). Scale bar, 100 μm. (**J**) High-magnification image of transplanted Wnt1-tdT$^+$ cells immunolabeled with TUBB3 in cross sections. Scale bar, 50 μm. (**K**) Images of whole-mount preparations of smooth muscle recipient tissues contained transplanted Wnt1-tdT$^+$ cells and neurons and nerve fibers immunoreactive for TUBB3. Scale bar, 500 μm. (**L** and **M**) Wnt1-tdT$^+$ cells (L) expressed TUBB3 (M) and formed ganglia-like structures (arrows) at the center of the transplantation site. Scale bars, 100 μm. (**N** and **O**) Representative images of transplanted Wnt1-tdT$^+$ cells immunolabeled for neuron-specific enolase (NSE) (N; scale bar, 50 μm) and expression of Tau^{GFP} (O; scale bar,

500 μm) in whole-mount preparations. (**P**) Representative image of the integration between transplanted Wnt1-tdT$^+$ cells and the endogenous enteric ganglia (arrows) expressing TUBB3. Scale bars, 50 μm. (**Q**) Immunohistochemical labeling of calretinin (Calr) in whole-mount preparations of the colon (scale bars, 500 μm). (**R** to **T**) Immunohistochemical labeling of neurochemical coding markers for calretinin (R), cholinergic (VAChT) (S), and neuropeptide Y (NPY) (T) expressing neuronal subtypes in cross sections of the colon. Scale bars, 50 μm. (**U**) Visualization of transplanted Wnt1-tdT$^+$ cells and immunohistochemical labeling of neuronal NOS (nNOS). Scale bar, 50 μm.

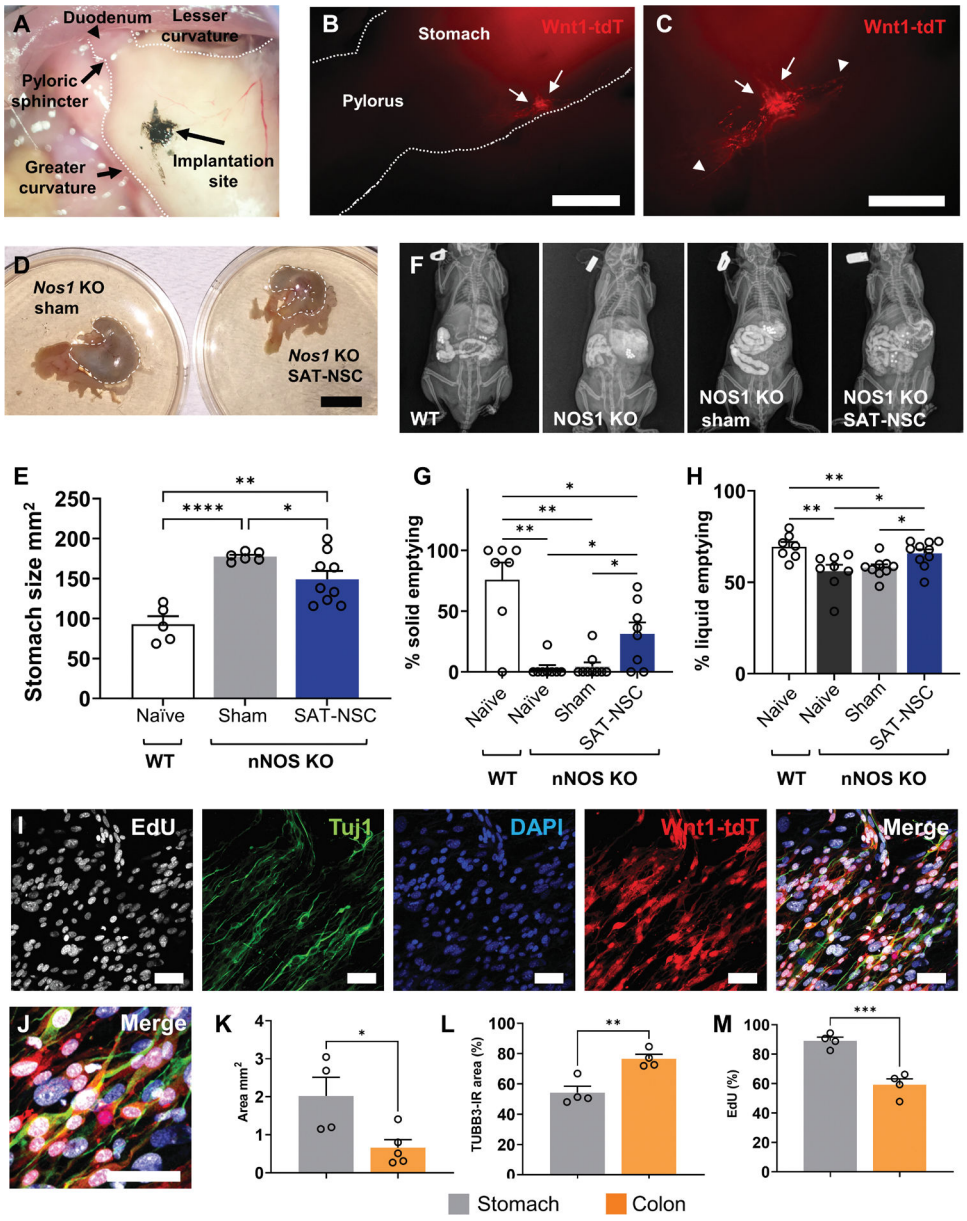

Fig. 5. Transplantation of SAT-NSCs alleviates gastroparesis in nNOS KO mice.

(**A**) Implantation of SAT-NSCs proximal to the pylorus in the stomach of the nNOS$^{-/-}$ mouse model of gastroparesis. (**B**) Engraftment of Wnt1-tdT^{+} SAT-NSCs (arrows) into the stomach. Scale bar, 2 mm. (**C**) SAT-NSCs with projecting nerve fibers (arrow heads) in the stomach. Scale bar, 1 mm. (**D**) Representative images of stomachs from nNOS$^{-/-}$ mice receiving implantation of SAT-NSCs and sham surgery and implantation controls. Scale bar, 1 cm. (**E**) Quantification of stomach sizes as area in mm^2. One-way ANOVA with Holm-Sidak multiple comparisons test, *$P < 0.05$, **$P < 0.01$, and ****$P < 0.0001$. Naïve wild-type (WT) mice, $n = 5$; sham nNOS$^{-/-}$, $n = 6$; and SAT-NSC–treated nNOS$^{-/-}$, $n = 9$ mice group. (**F**) Representative images of radiographic visualization of gavaged radiopaque beads and liquid barium in the gastrointestinal tract of naïve WT, nNOS$^{-/-}$, nNOS$^{-/-}$ mice with sham surgery, and nNOS$^{-/-}$ mice with SAT-NSC transplantation (left

to right). (**G**) Quantification of gastric emptying of solid materials (beads). Brown-Forsythe ANOVA test with Welch's corrected multiple comparisons *t* test, $*P < 0.05$ and $**P < 0.01$. Naïve WT mice, $n = 7$; naïve nNOS$^{-/-}$ mice, $n = 8$; sham nNOS$^{-/-}$, $n = 9$; and SAT-NSC–treated nNOS$^{-/-}$, $n = 8$ mice per group. (**H**) Quantification of gastric emptying of liquid materials (barium). Brown-Forsythe ANOVA test with Welch's corrected multiple comparisons *t* test, $*P < 0.05$ and $**P < 0.01$. Naïve WT mice, $n = 7$; naïve nNOS$^{-/-}$ mice, $n = 8$; sham nNOS$^{-/-}$, $n = 9$; and SAT-NSC–treated nNOS$^{-/-}$, $n = 8$ mice per group. (**I** and **J**) Representative single confocal slice images of EdU incorporation in proliferating cells, the neuronal marker TUBB3 (Tuj1), DAPI, Wnt1-tdT, and merged images (I, left to right, and J, magnified image) in the muscularis of the stomach ex vivo after Wnt1-tdT^{+} SAT-NSC implantation for 7 days. Scale bars, 50 μm. (**K** to **M**) Quantification of the total area (square millimeter) covered by migrating Wnt1-tdT^{+} SAT-NSCs (K), percentage of the TUBB3-immunoreactivity (IR) colocalization area with Wnt1-tdT^{+} SAT-NSCs (L), and the percentage of proliferating EdU^{+} SAT-NSCs (M) after 7 days in the stomach and colon. Unpaired *t* test, $*P < 0.05$, $**P < 0.01$, $***P < 0.001$, $n = 4$ mice per group.

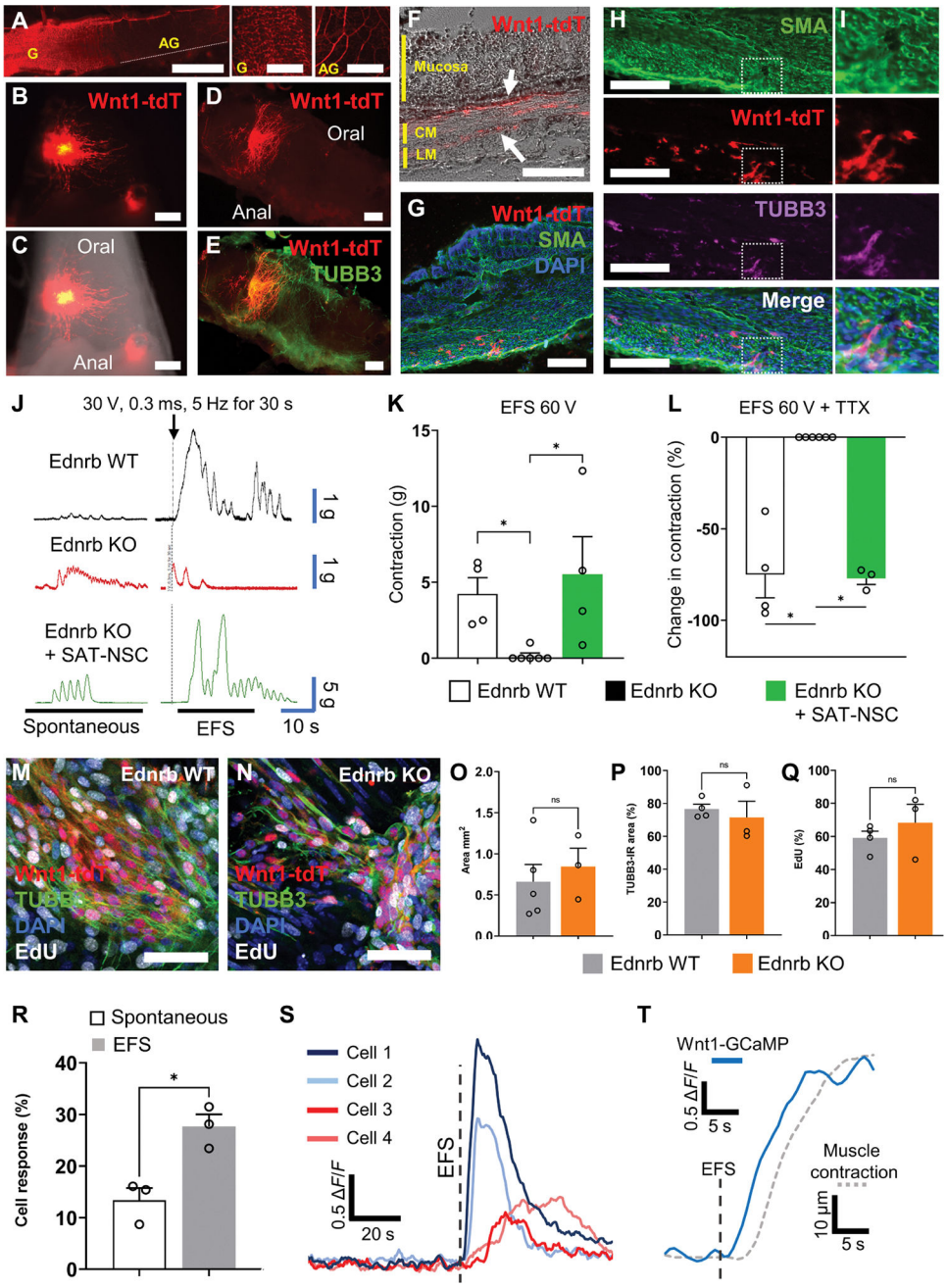

Fig. 6. SAT-NSCs restore muscle contraction in intestinal aganglionosis.

(**A**) Representative images of the nervous system in the colon of Wnt1-tdT;Ednrb KO mice. Scale bars, 4 mm. The proximal colon is ganglionated (yellow G) with intrinsic neurons, whereas the aganglionic (yellow AG) segment is observed from the mid colon to the rectum and contains only hypertrophic nerve fibers of extrinsic origin. Scale bars, 1 mm. (**B** and **C**) Expression of Wnt1-tdT in SAT-NSCs (B) 2 weeks after transplantation to the colorectum (C) of Ednrb$^{-/-}$ with colorectal aganglionosis at P6. Scale bars, 0.5 mm. (**D** and **E**) Images of whole-mount preparations of the Ednrb KO colon with transplanted Wnt1-tdT^{+} SAT-NSCs (D) and immunolabeled for the neuronal marker TUBB3 (E). Scale bars, 300

μm. (**F**) Cross section of the transplanted Ednrb KO colon in bright field. Arrows indicate transplanted Wnt1-tdT$^+$ cells located between the mucosa and circular muscle (CM) or the CM and longitudinal muscle (LM). Scale bar, 200 μm. (**G**) Cross section of the SAT-NSC transplanted Ednrb KO colon labeled for alpha smooth muscle actin (SMA) and stained with DAPI. Scale bar, 200 μm. (**H** and **I**) Representative images of the muscularis (SMA) in cross sections of the SAT-NSC transplanted Ednrb KO colon labeled with the neuronal marker TUBB3 (H, low magnification; I, high magnification). Scale bars, 200 μm. (**J**) Representative traces of colonic contractile force in Ednrb$^{+/+}$ (Ednrb WT, black), Ednrb$^{-/-}$ (Ednrb KO, red), and Ednrb$^{-/-}$ mice with SAT-NSC neurosphere implantation (Ednrb KO + SAT-NSC, green) before (spontaneous) and directly after EFS. (**K**) Quantification of the change in contractile force (grams) from baseline after EFS stimulation in Ednrb WT, Ednrb KO, and Edrnb KO mice after SAT-NSC transplants. Ednrb KO, $n = 6$; Ednrb WT and Edrnb KO + SAT-NSC, $n = 4$ mice per group. Kruskal-Wallis nonparametric ANOVA with Dunn's multiple comparisons test, $^*P < 0.05$. (**L**) Quantification of TTX-sensitive (neural) contributions to the EFS-induced contractile response. Ednrb WT, $n = 4$; Ednrb KO, $n = 6$; and Edrnb KO + SAT-NSC, $n = 3$ mice per group. Kruskal-Wallis nonparametric ANOVA with Dunn's multiple comparisons test, $^*P < 0.05$. (**M** and **N**) Representative single confocal slice images of EdU incorporation in proliferating cells (EdU) the neuronal marker TUBB3, DAPI, and Wnt1-tdT in the muscularis of the ganglionated Ednrb WT (M) and aganglionic Ednrb KO (N) distal colon after Wnt1-tdT$^+$ SAT-NSC implantation for 7 days. Scale bars, 50 μm. (**O** to **Q**) Quantification of the total area (square millimeter) covered by migrating Wnt1-tdT$^+$ SAT-NSCs (O), percentage of the TUBB3-immunoreactivity (IR) colocalization area with Wnt1-tdT$^+$ SAT-NSCs (P), and the percentage of proliferating EdU$^+$ SAT-NSCs (Q) after 7 days in the ganglionated (Ednrb WT) and aganglionic (Ednrb KO) colon. Ednrb WT, $n = 4$ and Ednrb KO, $n = 3$ mice per group, unpaired t test, NS, not significant. (**R**) Quantification of the number of spontaneous and EFS-invoked calcium responses in SAT-NSCs transplanted to the aganglionic colon. $n = 3$ per group, Unpaired t test, $^*P < 0.05$. (**S**) Representative traces of calcium transients ($\Delta F/F_0$) in transplanted SAT-NSCs in the aganglionic colon. Red traces denote neuronal-like responses to EFS, and blue traces denote glial-like secondary responses. (**T**) Representative traces of global calcium transients ($\Delta F/F_0$) from transplanted SAT-NSCs (solid blue) and smooth muscle contraction (dotted gray) in response to EFS in the aganglionic colon.

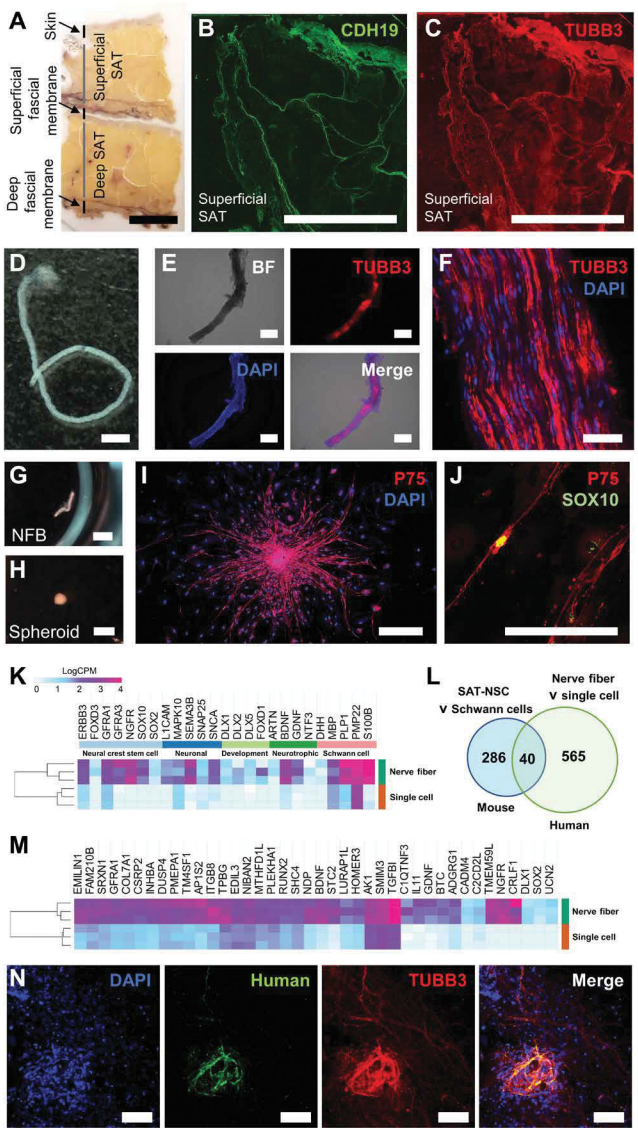

Fig. 7. Human adult SAT is a source of SAT-NSCs derived from NFBs.

(**A**) Sectional slice of resected human SAT. Scale bar, 1 cm. (**B** and **C**) Immunohistochemistry of the Schwann cell marker, CDH19 (B), and nerve fiber marker, TUBB3 (C), in cross sections of the superficial SAT. Scale bars, 1 cm. (**D**) Representative image of NFB isolated from digested SAT. Scale bar, 2 mm. (**E**) Representative images of bright field (top left), TUBB3 immunohistochemistry (top right), DAPI (bottom left), and merged images (bottom right) in a whole-mount NFB from the SAT. Scale bars, 500 μm. (**F**) High-magnification image of whole-mount NFB containing nucleated cells (DAPI) and expressing TUBB3. Scale bar, 50 μm. (**G** and **H**) Representative images of human SAT-derived NFB before (G; scale bar, 2 mm) and after culture (H; scale bar, 1 mm) in free floating conditions. (**I** and **J**) Representative images of immunohistochemical labeling for P75 (I; scale bar, 500 μm) and SOX10 (J; scale bar, 200 μm) in SAT NFB–derived spheroids cultured on fibronectin. (**K**) Heatmap representation of curated neural crest stem cell, neuronal, neural development, neurotrophic, and Schwann cell genes in SAT NFB–

derived spheroids compared to filtered single-cell suspension–derived spheroids visualized as LogCPM values. (**L**) Venn diagram of up-regulated genes common between human SAT NFB–derived spheroids compared to single-cell suspensions and mouse SAT-NSCs compared to Schwann cells. (**M**) Heatmap representation of common genes in SAT NFB–derived spheroids compared to filtered single-cell suspension–derived spheroids visualized as LogCPM values. (**N**) Representative image of human SAT NFB–derived cells labeled with TUBB3 after ex vivo transplantation. Scale bars, 200 μm.